Quaternary Science Reviews 270 (2021) 107179

Contents lists available at ScienceDirect

Quaternary Science Reviews

journal homepage: www.elsevier.com/locate/quascirev

Invited review

Pulsebeat of early Holocene glaciation in Baffin Bay from high-resolution beryllium-10 moraine chronologies

Nicolás E. Young [a, *], Jason P. Briner [b], Gifford H. Miller [c], Alia J. Lesnek [d, 1], Sarah E. Crump [c, 2], Simon L. Pendleton [e, 3], Roseanne Schwartz [a], Joerg M. Schaefer [a]

[a] Lamont-Doherty Earth Observatory, Columbia University, Palisades, NY, USA
[b] Department of Geology, University at Buffalo, Buffalo, NY, USA
[c] INSTAAR and Department of Geological Sciences, University of Colorado-Boulder, Boulder, CO, USA
[d] University of New Hampshire, Department of Earth Sciences, Durham, NH, USA
[e] Woods Hole Oceanographic Institution, Woods Hole, MA, USA

ARTICLE INFO

Article history:
Received 24 May 2021
Received in revised form
26 August 2021
Accepted 2 September 2021
Available online xxx

Handling Editor: C. O'Cofaigh

Keywords:
Cosmogenic nuclides
Greenland Ice Sheet
Laurentide Ice Sheet
Glaciers
North Atlantic
Meltwater
Bond events

ABSTRACT

Beryllium-10 has become the premiere cosmogenic nuclide for quantifying Earth-surface process. Routine measurement of ^{10}Be at the ≤ 2–3% precision level, coupled with precise ^{10}Be production-rate calibrations, now allow for ^{10}Be-based records of glacier and ice-sheet change to be reliably compared to independent records of climate variability. Here, we review efforts over the last 10+ years to characterize the Holocene behavior of ice sheets and glaciers fringing Baffin Bay using *in situ* ^{10}Be. Hundreds of ^{10}Be measurements present a detailed picture of ice-margin migration through the early Holocene. Widespread net deglaciation was interrupted by ice-margin readvances or stillstands, marked by modes of moraine deposition, near the end of the Younger Dryas (12.9–11.7 ka BP), 10.4–10.2 ka BP, 9.3 ka BP, and 8.2 ka BP, with perhaps additional widespread moraine deposition occurring ca. 9.7 ka BP and 7.3 ka BP. Modes of moraine deposition encompass independent and glaciologically distinct ice masses – the Greenland and Laurentide ice sheets and local alpine glaciers situated on Baffin Island and western Greenland – providing a robust, albeit discontinuous, record of widespread climatic changes in the Baffin Bay region in the early Holocene. Periods of glacier advance coincide with abrupt cooling events documented in Summit Greenland ice cores indicating that *i)* Baffin Bay ice masses largely followed the pattern of temperature change displayed in Greenland ice cores, *ii)* abrupt cooling events were of sufficient magnitude and duration to briefly synchronize the behavior of independent and glaciologically distinct ice masses across Baffin Bay despite varying degrees of dynamical influence, and *iii)* centennial-scale synchronization of ice masses requires that abrupt temperature changes recorded at Summit Greenland also occurred during the summertime within glacier ablation zones. Advancements in ^{10}Be methodology combined with an environment conducive towards developing ^{10}Be-based records of ice-margin change has resulted in ice-margin reconstructions that identify a potentially fundamental negative feedback mechanism inherent to melting ice sheets in the Baffin Bay region – elevated and episodic meltwater delivery into the Labrador Sea results in a decrease in the Atlantic meridional overturning circulation and regional cooling, which, in turn, drives a brief reversal of deglaciation. Under the right conditions ^{10}Be can be used to develop centennial-scale, climatically relevant records of glacier and ice-sheet change.

1. Introduction

Over the past three decades the cosmogenic isotope community has made significant methodological advances that have transformed our ability to characterize past changes in glacier dimensions (Granger et al., 2013; Balco, 2020). Pioneering efforts

* Corresponding author.
E-mail address: nicolasy@ldeo.columbia.edu (N.E. Young).
[1] Current Affiliation: School of Earth and Environmental Sciences, Queens College, City University of New York, New York, New York, USA
[2] Current Affiliation: Ecology and Evolutionary Biology, University of California Santa Cruz, Santa Cruz, CA, USA
[3] Current Affiliation: Environmental Science and Policy, Plymouth State University, Plymouth, NH, USA

https://doi.org/10.1016/j.quascirev.2021.107179
0277-3791/

applied ^{10}Be with sufficient resolution to distinguish between glacial landforms (i.e., moraines) deposited during Marine Isotope Stage (MIS) 6, MIS 2, and the late-glacial period (Gosse et al., 1995a, 1995b; Licciardi et al., 2001), whereas recent endeavors suggest that ^{10}Be can be used to develop records of glacier change that can be correlated to millennial- and even centennial-scale climate events recorded in independent archives (Schaefer et al., 2009; Kaplan et al., 2010; Putnam et al., 2012; Young et al., 2015, 2019; Levy et al., 2016; Marcott et al., 2019). Moraines are an attractive target for dating because they unequivocally mark past glacier extent and are globally distributed. As alpine glacier extent is driven almost exclusively by changes in only two variables – temperature and precipitation – records of glacier length serve as a relatively unambiguous proxy for past climate, although stochastic fluctuations in glacier length are perhaps possible in a stationary climate (e.g., Roe, 2011). Nonetheless, the strong relationship between glacier length and climate has placed a premium on characterizing the total uncertainties in ^{10}Be measurements needed to assess the feasibility of using ^{10}Be-dated moraines to develop millennial-to centennial-scale records of climate.

Much of the progress in ^{10}Be dating over the last few decades can be attributed to improvement in analytical capabilities. Typical ^{10}Be samples are now routinely measured at the $\leq$ 2–3% precision level (e.g., Rood et al., 2010, 2013) and, excluding geological uncertainties, this level of analytical precision theoretically allows for individually dated moraines to be correlated to millennial-scale climate events. For example, because measurements can be made with such a high degree of precision, it is often possible to develop moraine records within a single alpine valley where moraines that are relatively close in age can still be resolved with ^{10}Be (e.g., Putnam et al., 2012; Kaplan et al., 2013). Relying on a single ^{10}Be-dated moraine or suite of moraines from one location, however, could lead to spurious correlations between moraine ages and known climate events. To avoid this potential pitfall, arguments centered on the geographic expression of climate events should probably not be based on a single ^{10}Be-based record and instead ^{10}Be-based moraine chronologies should be replicated in several locations (Balco, 2020). For most applications in glacial settings, analytical errors are no longer the primary limiting factor in developing high-resolution ^{10}Be-based records of glacier change. Instead, difficult to quantify geologic-geomorphic uncertainties (e.g., Kelly et al., 2008; Crump et al., 2017) and systematic uncertainties (i.e., ^{10}Be production-rate calibrations and spatiotemporal scaling of ^{10}Be production), collectively referred to as total uncertainty, perhaps limit our ability to correlate moraines to climate events (Balco, 2020).

We can develop ^{10}Be-based records of glacier change that are resolved at millennial and centennial timescales, but it is unclear if these records can be confidently correlated to millennial- or centennial-scale climate events that are recorded in high-resolution climate archives (e.g., ice cores or speleothems). Key approaches toward characterizing the total uncertainty in ^{10}Be-based datasets and assessing their relationship to millennial- or centennial-scale climate events are to increase the number of records from a geographic region or geologic setting and develop robustly constrained local-to regional-scale ^{10}Be production-rate calibrations. Developing several ^{10}Be-based records from independent glaciers addresses concerns over record reproducibility, and systematic uncertainties on ^{10}Be ages should be minimized if measurements are made across several field sites within a particular region and if measurements from site to site have similar exposure durations. Coupling record reproducibility across a geographic region with local production-rate calibrations can lead to lower total uncertainties and facilitate a more straightforward comparison to independently dated climate archives. Several recent efforts have resulted in local-to regional-scale production-rate calibrations with $\leq$5% uncertainties (e.g., Balco et al., 2009; Putnam et al., 2010a; Kaplan et al., 2011; Young et al., 2013b; Kelly et al., 2015; Martin et al., 2015; Putnam et al., 2019) that have been strategically combined with large ^{10}Be-based datasets to link glacier change to millennial- and centennial-scale climate events (Putnam et al., 2010b; Garcia et al., 2012; Levy et al., 2016; Martin et al., 2020; Young et al., 2020a).

Here, we review ^{10}Be datasets developed over the last decade from several sites on Baffin Island and western Greenland that constrain the behavior of the Laurentide and Greenland ice sheets (LIS; GrIS) and independent alpine glaciers during the early Holocene, and we summarize decades of traditional radiocarbon constraints that preceded ^{10}Be-based chronologies. Additionally, we present new ^{10}Be ages from moraines deposited by two alpine glacier systems on the Cumberland Peninsula, Baffin Island (Fig. 1; Fig. 2). We couple these ^{10}Be-based datasets with radiocarbon constraints to outline how the chronology of moraine deposition and its climatic significance has evolved over the last several decades as the source of chronological constraints on ice-margin change has transitioned from radiocarbon to ^{10}Be measurements. Hundreds of ^{10}Be measurements from moraines deposited by the LIS, GrIS, and alpine glaciers across southwestern Greenland and Baffin Island, calculated with a regionally constrained ^{10}Be production-rate calibration, offer the opportunity to use an atypically large ^{10}Be dataset to 1) characterize ice-margin changes in Baffin Bay during the early Holocene, 2) determine if ^{10}Be-dated moraines can be correlated to millennial- and centennial-scale climate events, 3) assess the suitability of using several ^{10}Be-based moraine records in the aggregate to constrain regional climate dynamics in the early Holocene, and 4) evaluate the relationship between regional climate dynamics in the early Holocene defined by the regional moraine record and canonical records of early Holocene LIS discharge (i.e., Jennings et al., 2015) and North Atlantic Ocean circulation (i.e., Bond et al., 2001).

To help guide the reader, we outline the structure of manuscript. We first provide an overview of decades of radiocarbon constraints and ^{10}Be ages from Baffin Island and western Greenland and assess how these constraints have led to an evolving picture on the timing of moraine deposition from opposite sides of Baffin Bay. We next present new ^{10}Be ages from Baffin Island that constrain the timing of moraine deposition by alpine glaciers in the early Holocene. Our new ^{10}Be ages are combined with previously published ^{10}Be-based chronologies of ice sheet and glacier change fringing Baffin Bay to evaluate the timing of several ice-margin advances in the region through the early Holocene. Next, we use a combined chronology of ice-margin change in the Baffin Bay region to pinpoint intervals of regional cooling and their likely driving mechanisms. Lastly, we compare the timing of early Holocene glacier advances to the timing of Bond events and discuss their possible driving mechanisms, the phasing between the two, and how glacier advances and Bond events may be related.

1.1. Baffin Island: the moraine record and traditional radiocarbon constraints

Moraines dispersed across Baffin Island have long been of interest. Early reconnaissance work identified an extensive north-south trending moraine complex running parallel to the heads of east-west trending fiords dissecting Baffin Island (Ives and Andrews, 1963; Falconer et al., 1965; Blake, 1966). These moraines were deposited during the Cockburn Substage, originally defined between 9,000 and 8,000 ^{14}C yr BP (Miller and Dyke, 1974; Andrews and Ives, 1978). We acknowledge that because the Cockburn Substage is an interval of time, moraines of this era should technically

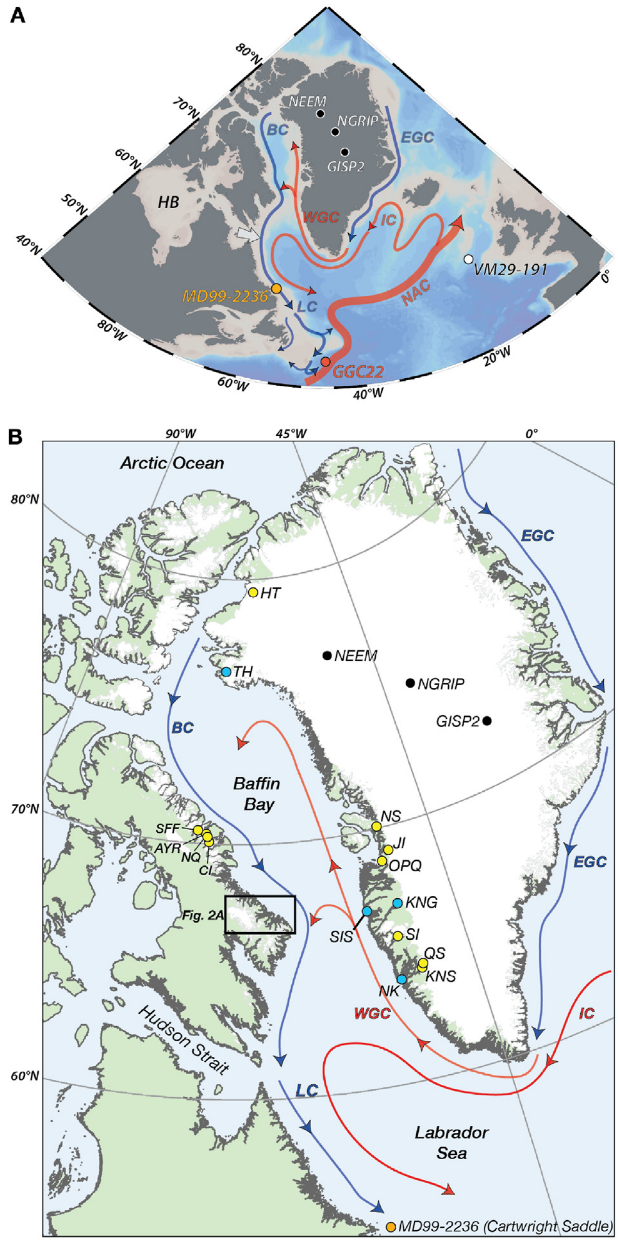

Fig. 1. (A) North Atlantic region with surface currents and marine core locations discussed in the text. NAC – North Atlantic Current, IC – Irminger Current, EGC – East Greenland Current, WGC – West Greenland Current, BC – Baffin Current, LC – Labrador Current. MD99-2236 (Jennings et al., 2015), GGC22 (Bond et al., 2001), VM29-191 (Bond et al., 2001). HB – Hudson Bay, and white arrow marks the Hudson Strait. (B) Baffin Bay region with early Holocene moraine chronologies discussed in the text (yellow dots) and place names (blue dots). SFF – Sam Ford Fiord, AYR – Ayr Lake valley, NQ – Naqsaq valley, CI – Clyde Inlet, NS – Nuusuaq, JI – Jakobshavn Isbræ, OPQ – Orpissoq, SI – Søndre Isortoq, QS – Qamanaarsuup Sermia, KNS – Kangiata Nunaata Sermia, KNG – Kangerlussuaq, HT – Humboldt glacier, SIS – Sisimiut, NK – Nuuk, TH – Thule.

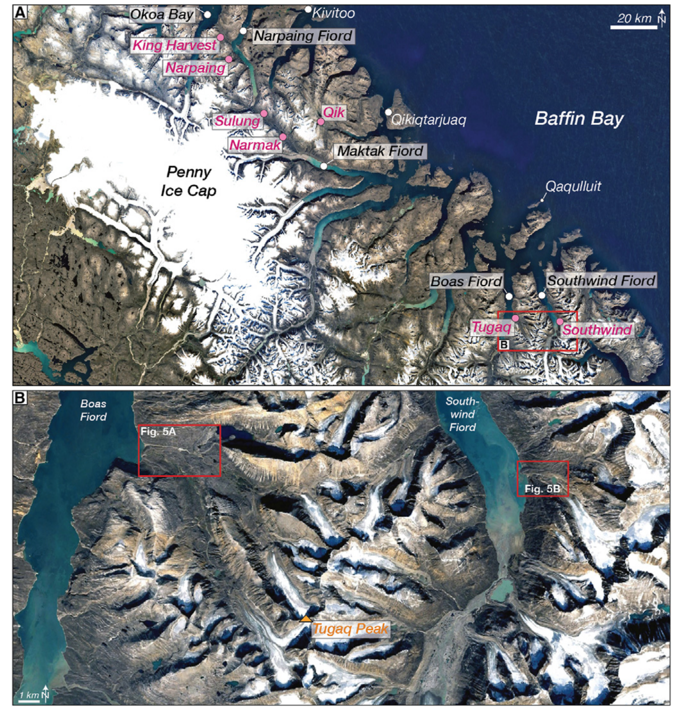

Fig. 2. (A) Cumberland Peninsula region with locations of ^{10}Be-dated early Holocene moraines (pink dots; Fig. 6) and the location of the Tugaq and Southwind field sites. Qikiqtarjuaq is the modern Inuit community whereas Kivitoo is a now abandoned Distant Early Warning line site. Qaqulluit can be seen in Fig. 8. (B) Southwind and Boas fiords with the locations of our target moraines (Fig. 5).

be referred to as "moraines of Cockburn age" and, in the strictest sense, any moraine not deposited between 9,000 and 8,000 ^{14}C yr BP should not be considered a moraine of Cockburn age. For simplicity and based on our updated review on the timing of early Holocene moraine deposition across Baffin Island presented here, we colloquially refer to these moraines as Cockburn moraines even if their age does not fall strictly between 9,000 and 8,000 ^{14}C yr BP; we refer to any moraine deposited during the early Holocene as a Cockburn moraine.

Cockburn moraines were initially thought to delimit the late Wisconsin maximum extent of the LIS based on their morphostratigraphic relationship to fossiliferous marine deposits; the Cockburn moraine system generally marks a boundary between raised marine sediments dated to <10,000 ^{14}C yr BP and >40,000 ^{14}C yr BP (Falconer et al., 1965; Miller and Dyke, 1974; Andrews and Ives, 1978; Ives, 1978). Moraines resting in alpine valleys located beyond the Little Ice Age/historical maximum moraine were thought to be Cockburn-equivalent features deposited by independent mountain glaciers or small ice caps (Andrews and Ives, 1978; Briner et al., 2009a). Offshore work in the 1990s in the Cumberland Sound, however, suggested that the LIS extended farther than previously thought during MIS 2 (Jennings, 1993; Jennings et al., 1996), which had also been previously proposed based on the overall magnitude of isostatic rebound in the region (Dyke, 1979). Strengthening the argument for a more extensive LIS were initial efforts using ^{10}Be in the early 2000s on Baffin Island to investigate LIS dynamics, which revealed that the Baffin sector of the LIS extended farther eastwards than previously thought and covered most of the eastern Baffin Island lowlands and extended out beyond the modern coastline during MIS 2 (e.g., Marsella et al., 2000; Kaplan et al., 2001; Miller et al., 2002; Briner et al., 2006; Davis et al., 2006). With these additional constraints revealing that the LIS covered most of Baffin Island and likely terminated in Baffin Bay during MIS 2, it thus became apparent that the Cockburn moraines were deposited during overall net retreat of the LIS from its MIS 2 maximum.

The precise chronology of early Holocene moraine deposition on Baffin Island, however, remained ambiguous. Until recently, almost all chronological constraints on the timing of moraine deposition were maximum- or minimum-limiting radiocarbon ages from bivalves found in raised marine deposits; there are relatively few direct age constraints (Andrews and Ives, 1978; Dredge, 2004; Briner et al., 2009a). In addition to these ages providing only maximum or minimum constraints, this typical sample setting presents two additional challenges: 1) radiocarbon ages from marine organisms are susceptible to often poorly constrained reservoir corrections, and 2) the relationship between the radiocarbon-dated material and a bonafide ice limit is sometimes unclear (Andrews and Ives, 1978). These limitations make it difficult to precisely constrain the timing of any single ice limit or to correlate ice limits across the region. An assortment of minimum-, maximum-limiting, and direct radiocarbon constraints span ~9.5 to 8.5 cal ka BP (n = 16; Fig. 3; Table 1; Andrews and Ives, 1978; Briner et al., 2009a).

Although the chronology of Cockburn moraine deposition has remained relatively unchanged over the last four decades, recent efforts have improved the chronological framework of Cockburn moraine deposition. In Clyde Inlet (Fig. 1), deposition of a Cockburn-aged ice-contact delta is constrained to ~8.4 to 8.0 cal ka BP based on bracketing radiocarbon ages. Of particular interest is that these radiocarbon constraints employ a locally constrained marine reservoir correction (Briner et al., 2007). In Sam Ford Fiord (Fig. 1), one fiord north of Clyde Inlet, this same locally constrained reservoir correction was applied to new and existing radiocarbon ages from marine bivalves associated with an ice-contact delta to constrain an advance of the Sam Ford Fiord outlet glacier to ~8.2 ka cal BP (Andrews and Drapier, 1967; Briner et al., 2009b).

1.1.1. ^{10}Be constraints

Most efforts to directly date early Holocene LIS or alpine limits have occurred on the Cumberland Peninsula (Fig. 1; Fig. 2). Bierman et al. (1999), Marsella et al. (2000), and Kaplan et al. (2001) presented dozens of ^{10}Be ages from the region that largely focused on LIS dynamics and the broad timing of deglaciation. Most relevant here, however, are ^{10}Be ages from boulders resting atop what are locally referred to as the Duval (and equivalent) moraines reported in Marsella et al. (2000) and re-interpreted by Corbett et al. (2016). Twelve ^{10}Be ages from moraine boulders are largely too old and likely pre-date the true timing of moraine deposition, but Corbett et al. (2016) suggested that the four youngest ^{10}Be ages could constrain moraine deposition to ca. 11.2 ka BP. In a similar fashion, Margreth et al. (2017) presented several new ^{10}Be ages across Cumberland Peninsula that broadly constrain the timing of regional deglaciation, but five ^{10}Be ages from moraine boulders across two separate moraines tentatively suggest episodes of moraine deposition occurred ca. 11.2 and 10.2 ka BP.

More recent efforts in the Cumberland Peninsula region have aimed to directly date several moraines deposited by the LIS and alpine ice. Young et al. (2020a) presented 61 ^{10}Be ages from the King Harvest site, which uniquely hosts moraines deposited by the LIS directly adjacent to moraines sourced from alpine ice. Combined, ^{10}Be ages revealed that LIS outlet glaciers and alpine ice advanced in unison ca. ~11.8–11.6, 10.4, and 9.3 ka BP. Crump et al. (2020) reported 33 ^{10}Be and 3 *in situ* ^{14}C ages from 6 moraines deposited by alpine ice at Narpaing, Sulung, and Narmak (Fig. 2) to constrain modes of alpine glacier advance to ca. 9 and 8 ka BP. Dated moraines from Crump et al. (2020) were interpreted as likely coeval with the 9.3 and 8.2 ka cooling events and synchronous with LIS and alpine advances reported in Young et al. (2020a).

In north-central Baffin Island, Briner et al. (2007) used ^{10}Be measurements from boulders atop an ice-contact delta at the head of Clyde Inlet to constrain a likely stillstand or readvance of the LIS in the early Holocene. Notably, this same ice-contact delta had existing radiocarbon constraints that allowed for the development of a locally constrained marine reservoir correction (see above), and when combined with ^{10}Be measurements, allowed for a local ^{10}Be production-rate calibration (Balco et al., 2009; see Section 2.3). Slightly north of Clyde Inlet in Ayr Lake, Young et al. (2012) used ^{10}Be to directly date adjacent moraines deposited by alpine ice to ~8.2 ka BP, which are thought to be equivalent to nearby fiord-head moraines (Fig. 1).

1.2. Western Greenland: the moraine record and traditional radiocarbon constraints

Moraines dispersed across western Greenland have been studied for decades (e.g., Weidick, 1968). The western margin of the GrIS terminated somewhere off the modern coastline during MIS 2 and moraines found across southwestern Greenland have classically been interpreted to represent stillstands or readvances of the ice margin during overall retreat from the LGM ice margin (Roksandic, 1979; Funder et al., 2011). Moraines generally span between ~64° and 70° N and are most concentrated in the Jakobshavn Isbræ (Sermeq Kujalleq) forefield, between Sisimiut and Kangerlussuaq, and in the Kangiata Nunaata Sermia (KNS) region east of Nuuk (Fig. 1). Of these regions, perhaps the most well-known moraines are the Fjord Stade moraines in the Jakobshavn Isbræ region (Fig. 1; Weidick, 1968). Early descriptions hypothesized that the Fjord Stade moraines were formed over a significant amount of time and could be divided into the outer Marrait and inner Tasiussaq moraine systems associated with marine limits of c. 75–65 and c. 45-40 m asl, respectively (Weidick, 1968; Kelly, 1985; Weidick and Bennike, 2007). Similar to the Cockburn moraines, the first chronological constraints were mainly radiocarbon ages from raised fossiliferous marine deposits. Radiocarbon ages from the eastern shores of Disko Bugt are generally between ~10 and 9 cal ka BP and serve as maximum-limiting ages for the Fjord Stade moraines, particularly the Marrait moraine system (Weidick, 1968, 1972a, 1973, 1974a, 1972a, 1974a; Weidick and Bennike, 2007). Unlike the chronological constraints on the Cockburn moraines, however, several radiocarbon ages from non-marine sources, mainly basal lake sediments, provide additional constraints on the timing of Fjord Stade moraine deposition. Between the Jakobshavn Isbræ region and Orpisoq to the south (Fig. 1) basal radiocarbon age from lakes located slightly inboard of the Tasiussaq moraine range from ~8.2 to 7.6 cal ka BP, with a single older age of ~8.8 cal ka BP (Fig. 3; Table 2; Long and Roberts, 2002; Long et al., 2006; Weidick and Bennike, 2007). Considering all of these radiocarbon ages constrains deposition of the Fjord Stade moraines to between ca. 10-8 cal ka BP.

Moraines between the present coastline and the modern ice margin in the Sisimiut-Kangerlussuaq region were initially described by Weidick (1974b) and Ten Brink (1975). This region is the widest ice-free section in Greenland allowing for the longest terrestrial-based chronology of ice sheet change. Here, the GrIS deposited several north-south trending moraine systems (listed oldest to youngest): Taserqat, Sarfartôq-Avatdleq, Fjord, Umîvît-Keglen, and Ørkendalen. Initial age constrains were, again, provided by radiocarbon ages from shells in raised marine deposits. Deglaciation of the outer coast is constrained by minimum-liming radiocarbon ages between ~11 and 10 cal ka BP. Additionally, a radiocarbon-dated local relative sea level curve combined with minimum-limiting radiocarbon ages from raised marine deposits constrain deposition of the Taserqat, Sarfartôq-Avatdleq, Umîvît-Keglen, and Fjord moraine systems to ca. >10.7, 9.8, 9.1, and 7.6 cal ka BP, respectively (Table 2; Ten Brink and Weidick, 1974; van Tatenhove et al., 1996). The Ørkendalen moraine system near Kangerlussuaq is particularly well-dated; radiocarbon ages from basal lake sediments within Ørkendalen drift constrain moraine deposition to ca. 7.3–7.0 cal ka BP (Fig. 3; Table 4; van Tatenhove

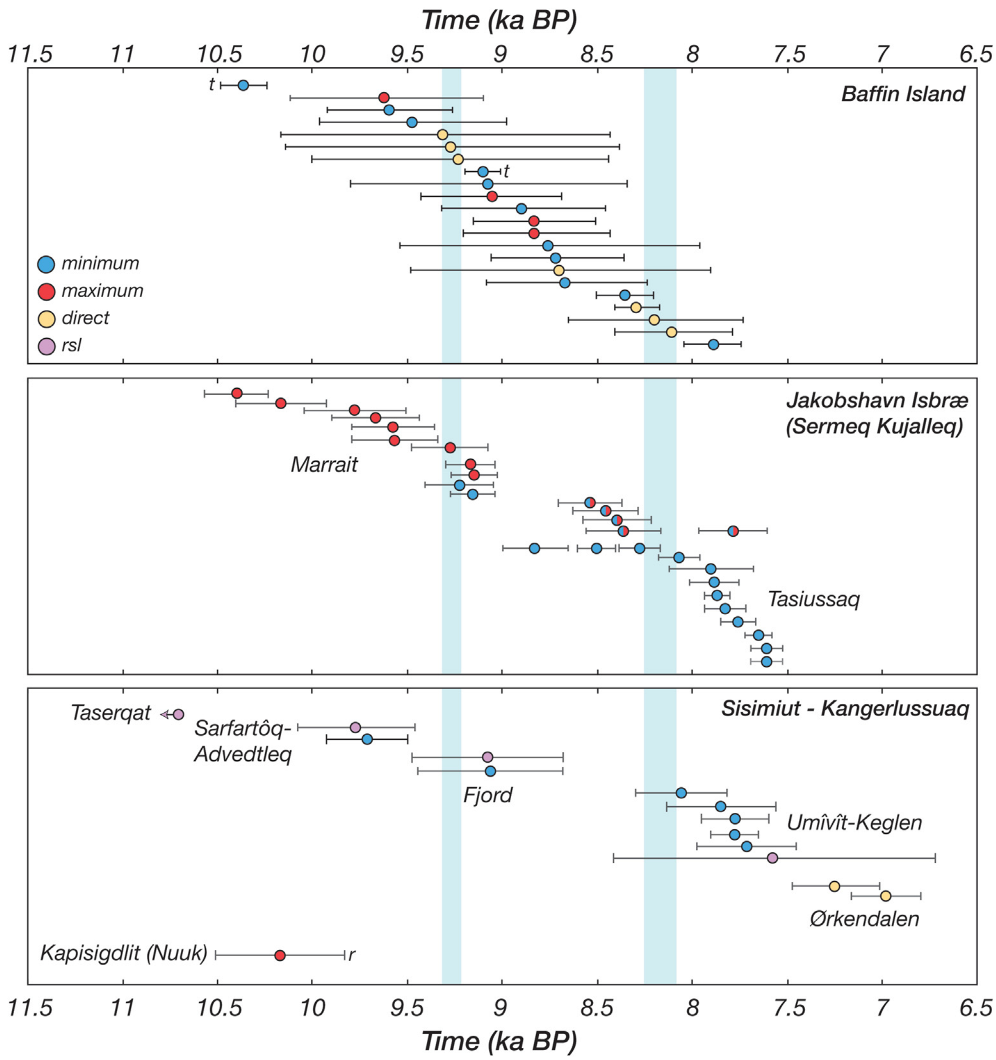

Fig. 3. Radiocarbon constraints on moraine deposition generated prior to the widespread use of ^{10}Be in the Baffin Bay region. Radiocarbon details are listed in Table 1 (Baffin Island) and Table 2 (Greenland); *t* marks a radiocarbon age from a terrestrial source. Radiocarbon ages are calibrated using Oxcal 4.4 and the INTCAL20 and MARINE20 databases (Bronk Ramsey, 2009; Reimer et al., 2020; Heaton et al., 2020) Shown are the median and 2σ calibrated age range. Blue shading marks the 9.3 ka BP and 8.2 ka BP cooling events.

et al., 1996). The Ørkendalen system comprises numerous moraine crests and radiocarbon ages are likely either maximum- or minimum-limiting constraints depending on which exact moraine crest the radiocarbon age is being compared to.

In the KNS region, the Kapisigdlit Stade moraine system is the most prominent feature marking a stillstand or readvance of the ice margin during overall deglaciation. Dozens of radiocarbon ages, marine and terrestrial, extending from the outer coast to just beyond the Kapisigdlit Stade moraine suggest that the moraine cannot be older than ca. 10.4 cal ka BP (Weidick, 1972b, 1975, 1975, 1976, 1975; Fredskild, 1983, Larsen et al., 2015). One estimate links the Kapisigdlit Stade moraine with a marine limit of 50 m asl, constraining deposition to ~8.3–8.1 cal ka BP (Weidick et al., 2012), whereas another estimate associates the Kapisigdlit Stade moraine with a marine limit between 100 and 80 m asl, placing the age of the moraine between ca. 10.1–9.6 cal ka BP (Larsen et al., 2015). The most direct age constraint is a maximum-limiting radiocarbon age from 10.17 ± 0.34 cal ka BP from reworked marine sediments indicating that deposition of the Kapisigdlit Stade moraine occurred via a readvance of the ice margin (Table 2; Weidick et al., 2012; Larsen et al., 2015).

1.2.1. ^{10}Be ages

Applications of ^{10}Be across western Greenland range from broad-scale deglaciation histories to efforts explicitly targeting the timing of moraine deposition. Here, we briefly outline, chronologically, the progression of ^{10}Be-based studies along western Greenland. The first applications of ^{10}Be in western Greenland helped constrain MIS 2 ice-sheet thickness and the general timing of deglaciation following the MIS 2 maximum extent (Rinterknecht et al., 2009; Roberts et al., 2009). Following these initial efforts, several studies have focused almost exclusively on pinpointing the timing of moraine deposition across western Greenland. Young et al. (2011a, 2011b, 2013a) combined direct ^{10}Be ages from moraine boulders and limiting ^{10}Be ages from immediately outside and inside well-preserved moraines in the Jakobshavn Isbræ forefield and at Orpissoq to constrain readvances of the GrIS to ca. 9.3 and 8.2 ka BP (Fig. 1). Notably, Corbett et al. (2011) reported maximum- and minimum limiting ^{10}Be ages on moraine deposition at Jakobshavn Isbræ that were statistically identical to those of Young et al. (2011a, 2011b), thereby increasing confidence in the ^{10}Be method and the ice-margin chronology at this site. To the south in the Kangerlussuaq region (Fig. 1), Levy et al. (2012) and Carlson et al. (2014) used ^{10}Be ages from moraine boulders to

Table 1
Radiocarbon ages from Baffin Island relating to Cockburn moraines.

Lab Number	Relationship to ice limit	Latitude (N)	Longitude (W)	Material Dated	Radiocarbon Age (14C yr BP)	Radiocarbon age uncertainty (yr; ± 1SD)	Calibrated Age (cal yr BP)	Calibrated ageuncertainty (2σ; yr)	Reference
I-1553	Ice contact	70.2100	71.2900	marine bivalves	7500	200	8200	460	Andrews and Draiper (1967)
CURL-7038	Ice contact/ minimum	69.8333	71.5000	marine bivalves	7620	40	7890	150	Briner et al. (2007)
Y-1834	Icecontact	68.6333	68.4000	marine bivalves	7820	140	8110	320	Andrews and Ives (1978)
GSC-1064	Unknown	71.4500	75.1333	marine bivalves	7890	160	8650	420	Andrews and Ives (1978)
I-1932	Minimum	69.8500	70.4667	marine bivalves	7940	130	8710	360	Andrews and Ives (1978)
I-1673	Minimum	69.6333	70.0333	marine bivalves	7970	340	8780	830	Andrews and Ives (1978)
SF07-SH01	Ice contact	70.2100	71.2900	marine bivalves	8000	20	8290	130	Briner et al. (2009b)
CURL-7046	Minimum	69.8500	72.5200	marine bivalves	8050	35	8350	150	Briner et al. (2007)
GSC-1060	Unknown	71.2576	73.7485	marine bivalves	8090	160	8890	440	Andrews and Ives (1978)
CURL-20189	Minimum - alpine	67.7266	65.5946	terrestrial moss	8130	25	9070	90	Crump et al. (2020)
I-1933	Maximum	70.3333	71.1333	marine bivalves	8210	130	9060	370	Andrews and Ives (1978)
GSC-462	Ice contact/ minimum	63.4248	68.4500	marine bivalves	8230	290	9080	740	Andrews and Ives (1978)
GaK-3092	Ice contact	67.9167	65.7500	marine bivalves	8290	340	8690	820	Andrews and Ives (1978)
I-724	Ice contact	72.0000	79.2500	marine bivalves	8350	300	9230	790	Andrews and Ives (1978)
GSC-1638	Ice contact	67.9333	66.0500	marine bivalves	8410	340	9310	900	Andrews and Ives (1978)
Y-1830	Ice contact/ maximum	68.9800	68.9800	marine bivalves	8430	140	8820	390	Andrews and Ives (1978)
GX-0930	Maximum	68.6333	68.4000	marine bivalves	8435	105	8820	320	Andrews and Ives (1978)
GSC-813	Ice contact/ maximum	68.9583	68.5667	marine bivalves	8630	190	9590	520	Andrews and Ives (1978)
GSC-2183	Ice contact/ minimum	66.5583	66.2667	marine bivalves	8660	110	9610	320	Andrews and Ives (1978)
St-3816	Ice contact	67.9500	65.7667	marine bivalves	8760	350	9250	910	Andrews and Ives (1978)
GaK-5479	Unknown	67.6167	65.1667	marine bivalves	8930	180	9450	490	Andrews and Ives (1978)
CURL-8272	Minimum- alpine	69.8166	69.1440	terrestrial plants	9170	25	10,310	110	Thomas et al. (2010)

Radiocarbon ages for terrestrial samples and are calibrated using Oxcal 4.4 and the INTCAL20 dataset (Bronk Ramsey, 2009; Reimer et al., 2020).
Marine samples are calibrated using Oxcal 4.4 and the MARINE20 database ($\Delta R = 0$; $R = 550$ years; Heaton et al., 2020). This resevoir correction is similar to the locally constrained resevoir correction of Briner et al. (2007; 540 years).
We added 400 years to older marine samples with I- and GSC- lab abbreviations because they were originally reported with an assumed $\delta^{13}C$ value of −25 per mille instead of 0 per mille.
Samples CURL-7038 and CURL-7046 (Briner et al., 2007) serve as bracketing ages for the Clyde Inlet ^{10}Be dataset (Fig. 6; Table S1).

directly date moraines within the Ørkendalen moraine complex to ca. 7.3–7.0 ka BP. In the KNS region, the first efforts using ^{10}Be did not date early Holocene moraines directly, but an extensive ^{10}Be dataset across the region was used in part to suggest that a prominent moraine in the KNS glacier forefield likely cannot be any older than ca. 10.4 ka BP (Larsen et al., 2015).

Building upon this initial wave of ^{10}Be-based moraine chronologies, Winsor et al. (2015) and Levy et al. (2018) directly, and independently, dated the same segments of the Keglen moraine to ca. 8 ka BP in the Kangerlussuaq region. Most recently in the Kangerlussuaq region, Young et al. (2020a) used 62 ^{10}Be ages to constrain episodes of moraine deposition by the GrIS to ca. 11.6, 10.4, 9.1, 8.1, and 7.3 ka BP. Cronauer et al. (2016) applied a limited ^{10}Be dataset to constrain the age of 3 moraines directly adjacent to the modern GrIS margin in central-west Greenland to ca. 8.6 to 7.6 ka BP, and at a nearby location, moraines deposited by alpine ice independent of the GrIS were robustly dated with ^{10}Be to ca. 10.4 ka BP (O'Hara et al., 2017). South of the Kangerlussuaq at Søndre Isortoq, Lesnek and Briner (2018) combined ^{10}Be ages from moraine boulders and boulders located immediately inboard and outboard of moraine segments deposited by the GrIS, to constrain intervals of moraine deposition at ca. 9.7 and 9.0 ka BP. In northwestern Greenland adjacent to Humboldt glacier (outlet glacier), ^{10}Be ages from a lateral moraine complex constrain moraine deposition to ca. 8.2 ka BP (Reusche et al., 2018). Lastly, Young et al. (2021) directly dated two prominent moraine segments deposited by the GrIS in the broader KNS region to ca. 10.2 and 9.6 ka BP.

1.3. Correlation of moraine systems on opposing sides on Baffin Bay

Hypotheses surrounding the correlation and climatic significance of moraines deposited across Baffin Island and western Greenland have evolved as chronologies of moraine deposition have been modified. Baffin Island's Cockburn moraines were initially linked to prominent moraine systems in the Keewatin and Labrador sectors (Falconer et al., 1965). In a similar fashion, Weidick

Table 2
Radiocarbon constraints on moraine depostion in western Greenland.

Lab Number	Latitude (N)	Longitude (W)	Material Dated	Radiocarbon Age (^{14}C yr BP)	Radiocarbon age uncertainty (±1σ; yr)	Calibrated Age (cal yr BP)	Calibrated age uncertainty (±2σ; yr)	Reference
Jakobshavn Isbræ (Sermeq Kujalleq)								
Fjord Stade moraines: maximum-limiting ages								
AA-37711	69.1757	51.8230	foraminifera	9485	65	10,170	220	Lloyd (2005)
AA-39655	68.6170	52.1103	basal lake sediments; bulk	9180	80	10,360	190	Long et al. (2003)
Ua-1086	69.2000	51.0667	marineshells	8795	65	9290	210	Weidick and Bennike (2007)
K-1818	69.1000	51.0667	marine shells	8630	65	9550	210	Weidick and Bennike (2007)
Ua-4574	69.0000	51.1167	marine shells	9180	75	9740	280	Weidick and Bennike (2007)
K-2023	69.0167	51.1333	marine shells	8680	70	9610	230	Weidick and Bennike (2007)
AA-39659	68.6674	51.1220	basal lake sediments; bulk	8585	86	9580	210	Long and Roberts (2002)
Maximum-limiting ages on Marrait moraine deposition								
CURL-11376	69.1088	51.0283	lake sediments; plant macrofossils	8225	20	9200	130	Young et al. (2011b)
CURL-11061	69.1088	51.0283	lake sediments; plant macrofossils	8180	25	9110	140	Young et al. (2011b)
Minimum-limiting ages on Marrait moraine deposition								
CURL-12594	69.1088	51.0283	lake sediments; plant macrofossils	8245	20	9210	130	Young et al. (2011b)
CURL-11374	69.1088	51.0283	lake sediments; plant macrofossils	8210	20	9180	140	Young et al. (2011b)
K-992	69.0333	51.0167	marine shells overlain by Tasiussaq outwash	7110	70	7790	190	Weidick and Bennike (2007)
K-993	68.9333	50.9667	marine shells overlain by Tasiussaq outwash	7650	70	8350	200	Weidick and Bennike (2007)
Ua-4575	69.0333	50.9333	marine shells overlain by Tasiussaq outwash	8140	50	8440	160	Weidick and Bennike (2007)
Ua-4573	68.9333	50.8833	marine shells overlain by Tasiussaq outwash	8215	40	8520	170	Weidick and Bennike (2007)
K-2022	69.0500	51.1333	marine shells overlain by Tasiussaq outwash	7690	60	8390	180	Weidick and Bennike (2007)
Beta-178168	69.1176	50.6333	basal lake sediments; bulk	7960	40	8830	200	Long et al. (2006)
Beta-178170	69.1235	50.5853	basal lake sediments; bulk	6910	40	7740	100	Long et al. (2006)
Beta-178169	69.1167	50.6167	basal lake sediments; bulk	6750	40	7610	70	Long et al. (2006)
Beta-178165	69.1220	50.6744	basal lake sediments; bulk	6760	40	7620	70	Long et al. (2006)
KIA-23028	69.4789	50.7051	basal lake sediments; bulk	6810	40	7640	70	Long et al. (2006)
OS-85087	68.6209	50.9593	basal lake sediments; plant macrofossils	7220	40	8020	120	Young et al. (2013a)
CURL-12698	68.6371	50.9840	basal lake sediments; plant macrofossils	7030	25	7870	80	Young et al. (2013a)
CURL-12693	68.6371	50.9840	basal lake sediments; plant macrofossils	6975	25	7810	100	Young et al. (2013a)
AA-39665	68.6375	50.9860	basal lake sediments; bulk; N3	7733	56	8510	110	Long and Roberts (2002)
AA-39664	68.6286	50.9587	basal lake sediments; bulk	7414	72	8240	180	Long and Roberts (2002)
AA-39661	68.6243	50.9352	basal lake sediments; bulk	7059	62	7880	130	Long and Roberts (2002)
Hel-369	68.6167	50.8667	marine shells	7210	85	7890	220	Donner and Junger (1975)
Sisimiut - Kangerlussuaq								
Taserqat moraine								
			RSL curve extraploation	≥9500		≥10,720		Ten Brink and Weidick (1974)
Sarfartôq-Advedtleq moraine system								
			RSL curve extraploation	8750	50	9690	220	Ten Brink and Weidick (1974)

(continued on next page)

Table 2 (*continued*)

Lab Number	Latitude (N)	Longitude (W)	Material Dated	Radiocarbon Age (^{14}C yr BP)	Radiocarbon age uncertainty (±1σ; yr)	Calibrated Age (cal yr BP)	Calibrated age uncertainty (±2σ; yr)	Reference
UW-172	66.6300	52.4200	marine shells	8670	100	9610	300	Ten Brink and Weidick (1974); van Tatenhove et al. (1996)
Fjord moraine								
			RSL curve extraploation	8250	150	9110	410	Ten Brink and Weidick (1974)
K-1663	67.0200	51.4000	marine shells	8230	140	9090	390	Ten Brink and Weidick (1974); van Tatenhove et al. (1996)
Umîvît-Keglen moraine								
			RSL curve extraploation	6900	400	7620	860	Ten Brink and Weidick (1974)
I-5512	67.0000	50.6900	marine shells; minimum-limiting age	7025	120	7710	260	Ten Brink and Weidick (1974); van Tatenhove et al. (1996)
UtC-3522	67.0000	50.6800	marine shells; minimum-limiting age	7500	70	7780	190	van Tatenhove et al. (1996)
CURL-11000	66.9782	50.9186	marine shells; minimum-limiting age	7625	15	7900	130	Storms et al. (2012)
AAR-3507	66.9883	50.6433	basal lake sediments; bulk; minimum-limiting age	7210	60	8020	140	Bennike (2000)
K-1664	67.0167	50.6833	marine shells; minimum-limiting age	7140	130	7820	290	Weidick (1972c); Bennike and Björck, 2002
Ørkendalen moraine system: direct								
Ut-1987	67.0900	50.2900	basal lake sediments within moraine system; bulk	6380	100	7300	220	van Tatenhove et al. (1996)
Ut-1990	67.0900	50.3400	basal lake sediments within moraine system; bulk	6090	50	6960	180	van Tatenhove et al. (1996)
Kapisigdlit moraine: maximum-limiting ages								
I-8565	64.3000	52.0667	Marine bivalve	9860	140	11,240	450	Weidick (1976)
I-8493	64.2200	51.9500	Marine bivalve	9460	140	10,680	440	Weidick (1976)
I-8566	64.3300	51.8800	Marine bivalve	9230	135	10,370	390	Weidick (1976)
I-8490	64.1200	51.7000	Marine bivalve	9355	140	10,530	430	Weidick (1976)
Ua-3476*	64.2800	50.1100	Marine bivalve; reworked	9490	105	10,170	330	Weidick (1972b); Weidick et al. (2012)

Radiocarbon ages for terrestrial samples and are calibrated using Oxcal 4.4 and the INTCAL20 dataset (Bronk Ramsey, 2009; Reimer et al., 2020).
Marine samples are calibrated using CALIB 8.2 and the MARINE20 database (ΔR = 0; R = 550 years; Heaton et al., 2020). We added 400 years to older marine samples with Hel-, I-, K-, and UW- lab abbreviations because they were originally reported with an assumed δ^{13}C value of −25 per mille instead of 0 per mille.
Samples CURL-12698, -12693, and AA-39665 are all basal radiocarbon ages from the same lake. CURL-samples are from macrofossils, whereas AA is from bulk sediments and appears to be slightly too old.
The extrapolated moraine ages from Ten Brink and Weidick (1974) are based on the elevational relationship between moraines and a radiocarbon-constrained relative sea-level curve. All of the original radiocarbon ages reported in Ten Brink and Weidick (1974; see their Table 1) used to construct the RSL curve are I-, K-, and UW- labeled marine shell samples that were reported with an assumed δ^{13}C value of −25 per mille instead of 0 per mille. The original authors then estimated the age of each moraine expressed as uncalibrated ^{14}C yrs BP (see Table 2 in Ten Brink and Weidick, 1974). To account for the assumed δ^{13}C values, we add 400 years to the moraine age estimates provided by Ten Brink and Weidick (1974), and then calibrate the ages as described above. I- samples in the Nuuk region are only loosely related to the Kapisigdlit moraine. These ages are minimum-limiting ages on the timing of coastal deglaciation located ~100 km west of the Kapisigdlit limit. Sample Ua-3476 is likely the only close radiocarbon constraint on the timing of moraine deposition; only Ua-3476 is shown in Fig. 3.

(1968) first suggested that moraines in southwestern Greenland marked the coeval behavior of different sectors of southwestern GrIS because moraines spanned at least 6 degrees of latitude. Building on these Canada- and Greenland-centric viewpoints, Ten Brink and Weidick (1974) argued that the simple existence of extensive moraine systems on opposing sides of Baffin Bay deposited by neighboring ice sheets suggested that these moraines were equivalent (synchronous) features because widespread climatic change was the only mechanism that could synchronize glaciers over such a large area. Moreover, these authors speculated that: 1) widespread readvances of the LIS and GrIS margins must have been driven by regional changes in summertime temperatures (versus precipitation) because only changes in temperature would be uniform over such a large area, and 2) based on preliminary δ^{18}O data emerging from the Camp Century ice core that revealed a climatically volatile early Holocene (i.e., Dansgaard et al., 1971), moraines could, in the future, potentially be correlated to specific changes in δ^{18}O seen in Greenland ice.

As the number of radiocarbon constraints relating to moraine systems on Baffin Island and western Greenland increased, the prevailing view shifted from moraines fringing Baffin Bay being equivalent features towards the asynchronous behavior of the LIS and GrIS during the early Holocene (Andrews and Ives, 1978). It was quickly realized that despite the sometimes-ambiguous relationship between radiocarbon-dated material and a paleo-ice limit on Baffin Island, the range in radiocarbon ages (~9.5–8.5 cal ka BP; Fig. 3) required that not all moraines were deposited at the same time and instead reflect numerous ice sheet advances (Andrews and Ives, 1978); dating and morphostratigraphic uncertainties likely cannot explain an ~1 kyr range in calibrated ages (Briner et al., 2009a). In western Greenland, maximum- and minimum-limiting radiocarbon ages also suggested that not all moraines were deposited in unison. If moraines segments within Baffin Island and western Greenland could not be correlated based on emerging chronological constraints (i.e., Long et al., 2006), then moraines systems could likely not be correlated across Baffin Bay. This transition from synchronous towards asynchronous moraine deposition occurred prior to the existence of high-resolution ice-core records from Summit Greenland. Without these now-canonical climate records, there were no known climate events in the region that could be invoked to synchronize the behavior of independent ice masses across Baffin Bay.

Hypotheses focusing on the role of dynamical processes and topography were instead used to explain the broad range in radiocarbon constraints. For example, in western Greenland, moraines appear to be more concentrated in regions dominated by topographically restricted fjords (Warren and Hulton, 1990). Here, moraine deposition would occur at topographic pinning points that would temporally stabilize the retreating ice margin, and applied at a larger scale, this hypothesis could explain the large range of radiocarbon constraints on both sides of Baffin Bay. With the establishment of Greenland ice-core records and the subsequent discovery of the 8.2 ka BP abrupt cooling event (Alley et al., 1997; Barber et al., 1999), however, there was renewed interest in relating the timing of moraine deposition to climate. Despite some radiocarbon constraints from western Greenland suggesting a possible link to the 8.2 ka event (e.g., Long and Roberts, 2002), highly resolved relative sea-level histories revealed that different moraine segments were associated with different marine limits and therefore moraines cannot be the same age (Long et al., 2006).

The idea that moraines on both sides of Baffin Bay might reflect the synchronous behavior of Baffin Bay ice masses, once again, became re-established with ^{10}Be-based chronologies. The first efforts using ^{10}Be to directly date moraines on Baffin Island and western Greenland perhaps shifted the focus back towards regional changes in climate – particularly the 8.2 ka event – as the primary driver of glacier behavior (Fig. 4; Young et al., 2011a, 2011b, 2012). Additional ^{10}Be datasets suggested a possible link between GrIS behavior and the 9.3 ka cooling event (Young et al., 2011b, 2013a, 2013a). Further proliferation of direct ^{10}Be-based moraine chronologies on Baffin Island and western Greenland suggested modes of moraine deposition at ca. 11.8–11.6 ka BP, 10.4–10.2 ka BP, 9.2–9.0 ka BP, and 8.2–8.0 ka BP (Winsor et al., 2015; Cronauer et al., 2016; O'Hara et al., 2017; Lesnek and Briner, 2018; Reusche et al., 2018, Crump et al., 2020; Young et al., 2020a), with perhaps additional modes of moraine deposition at 9.7–9.6 ka BP and 7.3–7.0 ka BP (Lesnek and Briner, 2018; Levy et al., 2012; Carlson et al., 2014; Young et al., 2020a, 2021). Although the link between the timing of moraine deposition and known cooling events at times other than ca. 9.3 and 8.2 ka BP is tenuous, synchronous moraine deposition at these times across Baffin Bay is suggestive of changes in regional climate driving synchronous ice mass behavior (Young et al., 2020a; see Section 5.2).

Despite changing viewpoints surrounding the climatic or non-climatic origins of moraines found on Baffin Island and western Greenland, driven by evolving ice-margin chronologies, a few clear themes have emerged: 1) moraine systems on both sides of Baffin Bay formed over a several-thousand-year window and were not deposited solely because of glacier response to any single climate event, 2) the relatively long period of moraine deposition does not necessarily preclude the synchronous behavior of Baffin Bay ice masses through the early Holocene (i.e., Andrews and Ives, 1978), and 3) glacier response to the 8.2 ka BP and 9.3 ka BP cooling events is likely part of the Baffin Island and western Greenland moraine systems with perhaps additional intervals of synchronous glacier behavior. Building on this decades-long progression of chronological constraints on Baffin Island and western Greenland moraine deposition, we present new ^{10}Be-dated records of glacier change from the Cumberland Peninsula, Baffin Island, that further add to the early Holocene evolution of glaciers and ice sheets in Baffin Bay. These new ^{10}Be ages are combined with the 10+ years of ^{10}Be-based direct moraine chronologies in Baffin Bay to generate a composite record of early Holocene glaciation that is compared to benchmark records of LIS behavior and meltwater production, regional climate, North Atlantic Ocean surface hydrography.

2. The Cumberland Peninsula and Naqsaq Valley, Baffin Island

2.1. Overview and setting

Located in southern Baffin Island, the Cumberland Peninsula is on the uplifted eastern rim of the Canadian Shield and hosts numerous independent ice caps and mountain glaciers, as well as the Penny Ice Cap, one of the few lasting vestiges of the LIS. Summer warming over the last few decades has driven sustained mass loss for glaciers and ice caps on Cumberland Peninsula (Gardner et al 2012; Miller et al., 2013). Originally, it was thought that much of Cumberland Peninsula escaped glaciation during the LGM (e.g., Miller and Dyke, 1974). Yet, studies employing radiocarbon-dated lake sediments and cosmogenic nuclides over the last few decades have revealed that most of Cumberland Peninsula was likely covered largely by cold-based ice during the LGM with fiords funneling warm-based, fast-flowing narrow ice outlets onto the continental shelf (Kaplan et al., 2001; Miller et al., 2002); perhaps only high elevation coastal peaks remained as nunataks (Miller et al., 2002; Margreth et al., 2016; Pendleton et al., 2019). Retreat of the LIS margin was interrupted by a series of stillstands or re-advances slightly prior to, or during the late-glacial period (Kaplan et al., 2001; Corbett et al., 2016; Margreth et al., 2017).

Boas and Southwind fiords are north-south trending fiords located southeast of the Penny Ice Cap (Fig. 2). During the LGM these fiords likely hosted outlets of a co-mingled Laurentide-alpine ice complex (e.g., Margreth et al., 2017), but today, neither fiord is occupied by ice. At the southern limit of the Southwind Fiord, an outlet glacier emanating from an alpine ice complex terminates at a large sandur (Fig. 2). Along each fiord are numerous alpine valleys trending perpendicular to the fiord axes, which host independent cirque glaciers or small outlets extending from upland ice fields (Fig. 2). At our Southwind and Boas fiord (hereafter referred to as the Tugaq Peak site) field sites, we targeted moraines resting in alpine valleys that are positioned beyond Little Ice Age/historical maximum moraines (Fig. 5). Historical moraines are easily identified by their generally close proximity to modern glacier termini, fresh nature, and lack of vegetation cover and soil development. Moraines thought to be of Cockburn age are located downvalley of historical moraines, have more subdued topography, and are much more vegetated. At the Tugaq Peak site, three coeval moraine sets are preserved on the landscape beyond historical moraines, each deposited by a separate alpine glacier (Fig. 5). Our target moraine set was deposited by alpine ice sourced from the south, and the end moraine at this site is linked to a submerged ice-contact delta at ~37 m bsl (Miller, 1975; Forbes et al., 2012; Cowan, 2015) At our Southwind Fiord site, one prominent set of lateral moraines are located beyond the historical moraines and grade to below present sea level.

Lastly, we present results from a separate area of central-east Baffin Island where targeted an early Holocene moraine in Naqsaq valley (alpine ice; Fig. 1). The full site description for the Naqsaq site can be found in Young et al. (2015), but the morphostratigraphic context is the same as our two Cumberland Peninsula sites: a moraine thought to be of Cockburn age located downvalley of the historical moraine. Notably, Naqsaq hosts a flight of late Holocene moraines that are dated with ^{10}Be to ~CE 1000-CE 1600 (Young et al., 2015).

2.2. Methods

Fieldwork on the Cumberland Peninsula was completed in CE 2015, and samples from Naqsaq valley were collected in CE 2013. Moraine crests were mapped prior to fieldwork and updated in the field. Samples for ^{10}Be dating were collected using a Hilti-brand AG500-A18 angle grinder-circular saw with diamond bit blades, and a hammer and chisel. Sample coordinates and elevations were collected with a handheld GPS device with a vertical uncertainty of $\pm$5 m, and GPS units were calibrated to a known elevation (sea level) each day. Topographic shielding was measured using a handheld clinometer.

We completed 28 new ^{10}Be measurements. All samples were processed at the Lamont-Doherty Earth Observatory (LDEO) cosmogenic dating laboratory following well-established protocols for quartz separation and Be isolation (Tables 3 and 4; Schaefer et al., 2009). We also report 2 ^{10}Be measurements that were completed in CE 2001 and only reported in Briner (2003); these samples were processed at the University of Colorado. AMS analysis was split between the Purdue Rare Isotope Measurement (PRIME) Laboratory ($n = 25$) and the center for Accelerator Mass Spectrometry at Lawrence Livermore National Laboratory (LLNL-CAMS; $n = 5$). All LDEO processed samples collected during the CE 2013 and 2015 field seasons were measured relative to the 07KNSTD standard with a ^{10}Be/^{9}Be ratio of 2.85×10^{-12} using a ^{10}Be half-life of 1.387 Ma, and the 1σ analytical error ranged from 1.9% to 6.6% with an average of 3.6 $\pm$ 1.0% (Nishiizumi et al., 2007; Chmeleff et al., 2010, Table 3). The two older samples from CE 2001 were measured at LLNL-CAMS relative to KNSTD and have 1σ analytical errors of 5.8% and 8.8%, respectively (Table 3). Process blank corrections were applied by using the batch-specific blank value, expressed as number of atoms, and subtracting this value from the sample atom count (Table 4). We propagate through a 1.5% uncertainty in the carrier concentration when calculating ^{10}Be concentrations.

New and previously published ^{10}Be ages are calculated using the Baffin Bay ^{10}Be production-rate calibration dataset (Young et al., 2013b). Ages are reported using the time-variant 'Lm' scaling (Lal, 1991; Stone, 2000), which accounts for changes in the magnetic field although these changes are minimal at the high latitudes considered here. All ages are calculated in *MATLAB* using code from version 3 of the exposure age calculator found at https://hess/ess/washington.edu/, which implements an updated treatment of ^{10}Be production by muons (Balco et al., 2009; Balco, 2017). We do not correct nuclide concentrations for snow-cover or subaerial surface erosion because samples are primarily from windswept locations (moraine crests) and many surfaces still retain primary glacial features. Our group has collected many samples for ^{10}Be dating on Baffin Island in the spring, the time of maximum snow cover in the region, and we have not observed any significant snow accumulation on boulder surfaces. We do not correct the potential effects of isostatic rebound on nuclide production because the production-rate calibration sites and the sites of unknown age presented here, as well as ^{10}Be ages reviewed below, have experienced similar exposure and uplift histories (see Young et al., 2020a, 2020b; see Section 2.3). Individual ^{10}Be ages are first presented and discussed with 1σ analytical uncertainties and moraine ages do not include the ^{10}Be production-rate uncertainty when comparing ages of ^{10}Be-dated moraines across Baffin Bay. When moraine ages are compared to independent climate records, we propagate through the production-rate uncertainty (1.8%) in quadrature. All ^{10}Be ages are presented in thousands of years BP (CE 1950); exposure ages relative to the year of sample collection are reported in Supplementary Tables 1 and 2

2.3. Using the Baffin Bay ^{10}Be production-rate calibration dataset

Absolute ^{10}Be ages that can be directly compared to Greenland ice core records or marine archives rely on which production-rate calibration is used to calculate ^{10}Be ages. Several production-rate calibrations now exist (e.g., Balco et al., 2009; Putnam et al., 2010a; 2019; Kaplan et al., 2011; Borchers et al., 2016), but the Baffin Bay production-rate calibration includes several local to regional considerations that likely make it the most appropriate calibration for the Baffin Bay region (Young et al., 2013b). A subset of ^{10}Be ages in the Baffin Bay region are uniquely intertwined with the Baffin Bay ^{10}Be production-rate calibration. Initially, it was noted that ^{10}Be ages in the Jakobshavn Isbræ region were inconsistent with existing radiocarbon constraints when calculated using a global calibration dataset. Instead, use of the lower northeastern North America production-rate calibration dataset yielded older ^{10}Be ages (NENA; Balco et al., 2009) that satisfied radiocarbon constraints (Briner et al., 2012). Following this effort, the existing radiocarbon constraints and ^{10}Be concentrations from the Jakobshavn Isbræ region discussed in Briner et al. (2012) were re-cast as a production-rate calibration dataset linked to the Tasiussaq moraine (Fig. 4). This calibration was combined with 1) a calibration dataset from Baffin Island that was included within the NENA dataset, but where the ^{10}Be concentrations were remeasured with higher precision (Clyde Inlet; Fig. 6), and 2) a second calibration dataset from Jakobshavn Isbræ based on new radiocarbon constraints and ^{10}Be measurements linked to the Marrait moraine (Young et al., 2013b). These three calibration datasets were subsequently combined to generate the Baffin Bay production-rate calibration dataset (18 ^{10}Be measurements and 24 ^{14}C constraints in total).

Key to the merged Baffin Bay production-rate calibration dataset is that it is weighted towards the Marrait moraine calibration. The Marrait calibration dataset offers measured ^{10}Be concentrations with minimal scatter ($n = 5$), coupled with the most well-constrained independent (radiocarbon) age for the geological feature targeted among the three calibration datasets (Young et al., 2013b). Using the Baffin Bay production-rate calibration in the immediate Jakobshavn Isbræ region, however, introduces some degree of circularity where moraines dated with radiocarbon to ~9.3 ka BP and ~8.2 ka BP are used to develop a ^{10}Be production-rate calibration, which is in turn used to ^{10}Be date these same moraines to ~9.3 ka BP and 8.2 ka BP (albeit with additional samples). We note, however, that the Marrait and Tasiussaq moraines can likely be constrained to 9.3 ka and 8.2 ka BP based on the radiocarbon constraints alone (Fig. 4). In addition, use of the statistically identical NENA production-rate calibration (Balco et al., 2009), which does not include the calibration datasets from Jakobshavn Isbræ region, or the recent high-latitude calibration from the Scottish

Highlands that yields a comparable production rate (Putnam et al., 2019), would result in nearly identical ^{10}Be ages for not only the Jakobshavn Isbræ region, but across Baffin Bay.

To a lesser extent, ^{10}Be ages from Clyde Inlet are susceptible to circularity where a ^{10}Be production-rate calibration is then used to constrain the age of the ice-contact delta. The calculated ^{10}Be age of the ice-contact delta (Table S1; Fig. 6), however, is based on the Baffin Bay calibration, which is, again, strongly weighted towards the Marrait calibration dataset. Rather, the Clyde Inlet production-rate calibration samples do not dominate the calculated ^{10}Be age of Clyde Inlet ice-contact delta and use of recent high-latitude production-rate calibrations would result in nearly identical ^{10}Be ages. To summarize, in the strictest sense, the Baffin Bay ^{10}Be production-rate calibration may not be appropriate for constraining the ages of early Holocene moraines in the Jakobshavn Isbræ forefield with ^{10}Be but substituting in any of these well-constrained high-latitude production-rate calibrations will result in statistically identical ^{10}Be ages. Across the broader Baffin Bay region, however, where there are no links or minimal links (Clyde Inlet) between the production-rate calibration and existing radiocarbon constraints, the Baffin Bay calibration can be applied without reservation (Fig. 4; Fig. 6; Fig. 7).

Applying the Baffin Bay calibration across the broader Baffin Bay region offers perhaps a few advantages over alternative calibrations. In general, the exposure duration of the calibration sites is comparable to sites of unknown age (up to ~9.2 kyr), and because the calibration sites and unknown sites are from high latitude, uncertainties in the scaling of ^{10}Be production with latitude are likely minimal. In other words, the calculated Baffin Bay sea-level/high-latitude (SLHL) production-rate calibrations are derived from SLHL locations. Calibration datasets from higher elevations or lower latitudes must be scaled to SLHL, which could incorporate geographical scaling errors if applied in Baffin Bay. In addition, the Baffin Bay calibration sites underwent varying degrees of isostatic rebound following local deglaciation. Although the competing effects of rebound and redistribution of atmospheric pressure are difficult to properly quantify (e.g., Staiger et al., 2007; Young et al., 2020b), these outstanding uncertainties are indirectly accounted for as sites of unknown age in Baffin Bay have, with few exceptions, undergone similar amounts of isostatic rebound as the calibration sites (Young et al., 2020b).

The uncertainty in a reference production rate establishes absolute uncertainties on a ^{10}Be moraine chronology and allows for direct comparison to independent climate archives. The primary drawback of using regional or local ^{10}Be production-rate calibration datasets is the risk of incorporating an artificially low production-rate uncertainty into the age of a ^{10}Be-dated feature. By their very nature, local and regional calibrations typically contain a smaller number of calibration datasets than larger compilations and thus the minimal scatter in ^{10}Be measurements and typical high precision in regional calibration datasets may simply be an artifact of fewer data (Balco, 2020). As mentioned above, the Baffin Bay calibration comprises three independent datasets and does not just rely on a single calibration dataset. The stated uncertainty in the Baffin Bay calibration is 1.8% (Young et al., 2013b) and although this uncertainty is lower than the uncertainties of other individual production-rate calibrations, it could be considered a conservative value as the weighted mean used to arrive at this value results in a higher uncertainty than taking a straight mean of all three calibration datasets (Young et al., 2013b). While we do not advocate for combining regional calibrations, other high-latitude calibrations (NENA; Scottish Highlands) are statistically identical to the Baffin Bay calibration, and if combined with the Baffin Bay calibration, a back-of-the-envelope calculation results in a production rate that is only ~1% lower with an uncertainty of <2%.

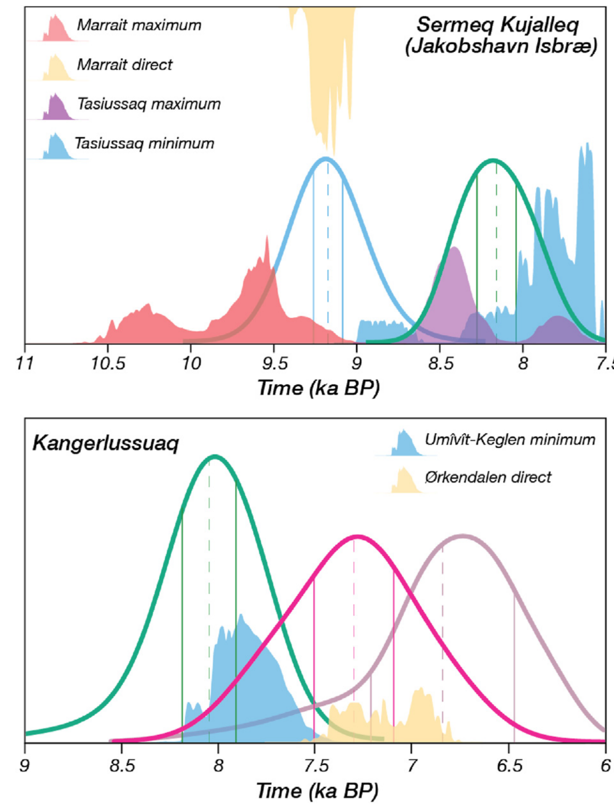

Fig. 4. Relationship between ^{10}Be ages and radiocarbon ages at two sites in southwestern Greenland. At Sermeq Kujalleq (Jakobshavn Isbræ), ^{10}Be ages from the Marrait (blue) and Tasiussaq (green) moraine are consistent with bracketing radiocarbon constraints. The Baffin Bay ^{10}Be production-rate calibration used to calculate ^{10}Be ages relies on the direct radiocarbon constraints for the Marrait moraine (Young et al., 2013b); ^{10}Be ages from the Marrait moraine shown here are the actual production-rate calibration samples. Using an alternative high-latitude production-rate calibration such as the NENA (Balco et al., 2009) or Scottish Highlands calibrations (Putnam et al., 2019), would yield ^{10}Be ages that vary by <2% and still satisfy the radiocarbon constraints (e.g., Briner et al., 2012). In the Kangerlussuaq region, ^{10}Be ages are consistent with limiting radiocarbon ages. ^{10}Be ages from the Umîvît-Keglen moraine includes those from Winsor et al. (2015), Levy et al. (2018), and Young et al. (2020a). The exact relationship between the Ørkendalen radiocarbon constraints and ^{10}Be ages is slightly ambiguous. Based on their location and original description (van Tatenhove et al., 1996), they are likely contemporaneous or minimum age constraints for the ^{10}Be ages presented in Young et al. (2020a) from the outer Ørkendalen moraine (magenta). These same radiocarbon ages are likely maximum ages for the moraine crests sampled by Levy et al. (2012) and Carlson et al. (2014), which are inboard of the outer Ørkendalen limit sampled by Young et al. (2020a); ^{10}Be ages presented in Levy et al. (2012) and Carlson et al. (2014) shown in light purple. Although there are several radiocarbon constraints related to early Holocene moraine deposition on Baffin Island (Fig. 3; Table 1), these constraints are geographically scattered and rarely paired with robust ^{10}Be datasets; the exception is the Clyde Inlet dataset (see Table 1 and Fig. 6). Details for radiocarbon and ^{10}Be ages can be found in Table 2 and S1.

3. Results

Eleven ^{10}Be ages from our Tugaq Peak site (Boas Fiord) range from 29.70 ± 0.88 ka BP to 7.08 ± 0.26 ka BP (Fig. 5; Table 3). Three of these ^{10}Be ages are from boulders perched on bedrock surfaces located outboard of our target moraine and have overlapping ^{10}Be ages at 1σ uncertainties of 12.58 ± 0.39 ka BP, 12.35 ± 0.45 ka BP, and 12.06 ± 0.40 ka BP. Combined, these ^{10}Be ages average 12.33 ± 0.26 ka BP, which serves as a maximum-limiting age for our target moraine. ^{10}Be ages for moraine boulders range from 29.70 ± 0.88 ka BP to 7.08 ± 0.26 ka BP, but we calculate an arithmetic mean age of 9.21 ± 0.34 ka (n = 6) after discarding a single

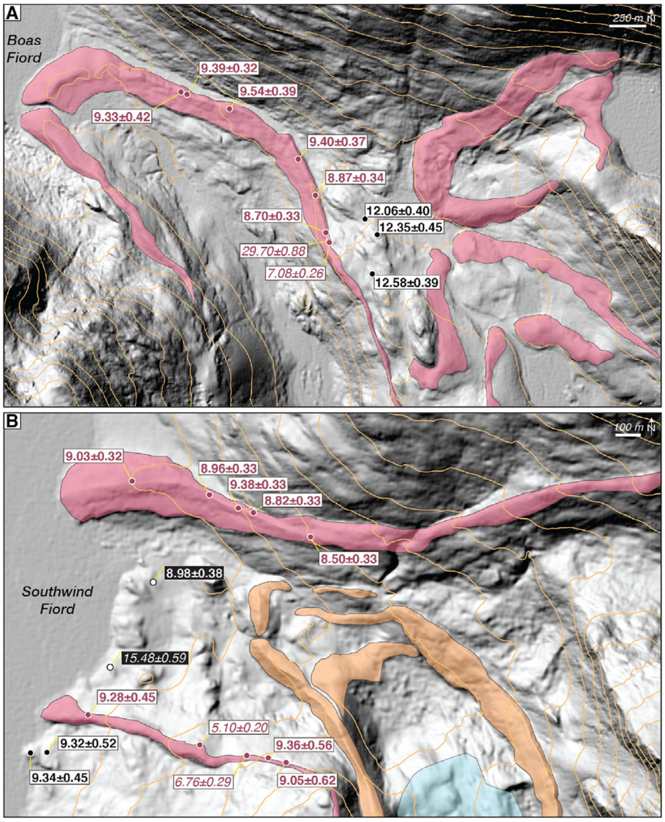

Fig. 5. (A) Tugaq peak field site at Boas Fiord with pre-Little Ice Age moraines preserved on the landscape (pink). ^{10}Be ages are shown in two morphostratigraphic groups (ka BP ± 1σ analytical uncertainty; outliers are in italics): 1) outboard of the target moraine, which serve as maximum-limiting ages on the moraine (black text), and 2) moraine boulders (red). (B) Southwind Fiord site with a pre-Little Ice Age moraine (pink), the Little Ice Age moraine (orange) and the modern glacier. Little Ice Age moraines on Baffin Island are easily identifiable via their position as typically the first moraine in front of modern glacier termini and their unvegetated nature. ^{10}Be ages are shown in three morphostratigraphic groups: 1) outboard of the target moraine (black text), which provides a maximum-limiting age on the target moraine and constraints the timing of deglaciation of ice through Southwind Fiord, 2) moraine boulders (red), and 3) inboard of the target moraine, which serve as minimum-limiting ages on the moraine (white text). Contour interval is 50 m.

older outlier (29.70 ± 0.88 ka BP) and a single younger outlier (7.08 ± 0.26 ka BP; Fig. 4). The older outlier is > 2σ older than the mean of the remaining ^{10}Be ages, pre-dates the LGM, and is likely influenced by isotopic inheritance. The younger outlier is > 2σ younger than the mean of the remaining ^{10}Be ages and is likely influenced by some degree of boulder exhumation. Excluding these two outliers, our ^{10}Be ages reveal that initial site deglaciation occurred at 12.33 ± 0.26 ka, followed by a glacier readvance culminating at 9.21 ± 0.34 ka BP (Fig. 5; Fig 6).

At Southwind Fiord, ^{10}Be ages range from 15.48 ± 0.59 ka BP to 5.10 ± 0.20 ka BP (n = 14; Fig. 5; Table 3). Two ^{10}Be ages from boulders perched on bedrock located outboard of our target moraine are 9.34 ± 0.45 ka BP and 9.32 ± 0.52 ka BP, and likely provide a robust maximum-constraining age on the timing of moraine deposition (Fig. 5). Ten ^{10}Be ages from moraine boulders have a mean age of 9.05 ± 0.30 ka BP after excluding two younger outliers of 6.76 ± 0.29 ka BP and 5.10 ± 0.20 ka BP that are >2σ younger than the mean ^{10}Be age and are likely influenced by boulder exhumation. Two ^{10}Be ages from boulders perched on bedrock located immediately inboard of the moraine are 15.48 ± 0.59 ka BP and 8.98 ± 0.38 ka. The older of these two ^{10}Be ages is older than any other ^{10}Be age in our Southwind Fiord dataset, including those from the morphostratigraphically older moraine and landscape located beyond the moraine; this ^{10}Be age is likely influenced by isotopic inheritance. The younger ^{10}Be age of 8.98 ± 0.38 ka is statistically identical to the direct moraine age of 9.05 ± 0.30 ka BP and serves as a minimum-limiting age on the moraine. Excluding three outliers, ^{10}Be ages from our Southwind Fiord site reveal that LIS-sourced ice in the main fjord retreated behind the alpine valley mouth ca. 9.4–9.3 ka BP, which also represents a maximum-limiting age on moraine deposition, followed by moraine deposition at 9.05 ± 0.30 ka BP and retreat shortly thereafter.

At Naqsaq valley, five ^{10}Be ages from moraine boulders are 25.58 ± 2.88 ka BP, 10.27 ± 0.25 ka BP, 10.27 ± 0.25 ka BP, 10.05 ± 0.27 ka BP, and 9.57 ± 1.14 ka BP (Table 3). The oldest age is almost certainly influenced by isotopic inheritance as it is much older than the timing of local deglaciation that occurred ca. 10–8 ka BP (i.e., Briner et al., 2007). The remaining ages all overlap at 1σ uncertainties, but the age of 9.57 ± 1.14 ka BP, measured in CE 2001, has a significantly larger analytical uncertainty than our more recent samples. To account for this larger uncertainty from a prior generation of ^{10}Be analysis, we calculate a weighted-mean age of 10.19 ± 0.25 ka as best estimate for the timing of moraine deposition (Table 3; Fig. 6).

4. Timing of moraine deposition across Baffin Bay

^{10}Be measurements from eighteen sites across Baffin Island and western Greenland constrain advances of the LIS, GrIS, and independent alpine glaciers on Baffin Island and western Greenland through the early Holocene (Fig. 6; Fig. 7; see captions for full citation list). On the Cumberland Peninsula, our new ^{10}Be ages reveal that alpine moraines at the Tugaq Peak and Southwind Fiord sites are coeval features with glacier advances culminating at 9.21 ± 0.34 ka BP and 9.05 ± 0.30 ka BP, respectively (Fig. 6). Across 11 sites on Baffin Island with ^{10}Be dated moraine systems, 5 of them record culminations of both alpine glacier and LIS advances centered at ~9.2–9.0 ka BP (Fig. 6; Table S1). Additional modes of moraine deposition on Baffin Island occur ca. 11.8–11.6 ka BP (1 site; Fig. 6), ca. 10.3–10.2 ka BP (2 sites, including the newly dated Naqsaq site), and 8.2–8.0 ka BP (4 sites; Fig. 6). The King Harvest site on the Cumberland Peninsula appears to record the most detail on Baffin Island hosting moraines dated to ~11.8–11.6 ka BP, 10.4–10.2 ka BP, and 9.2–9.0 ka BP, but lacks the 8.2–8.0 ka BP mode of moraine deposition seen at other sites on Baffin Island (Young et al., 2020a). No single site on Baffin Island contains each pulse of moraine deposition as defined by the collective ^{10}Be-dated moraine record, but no matter the number of moraines preserved at each site, each dated moraine falls into a well-defined mode of moraine deposition when considering the entire Baffin Island dataset (Fig. 6).

The record of moraine deposition in western Greenland is similar to that of Baffin Island (Fig. 7). ^{10}Be ages from eight sites in western Greenland constrain advances of the GrIS and alpine glaciers at ca. 11.6 ka BP (1 site), 10.4–10.2 ka BP (3 sites), 9.7–9.6 ka BP (2 sites), 9.2–9.0 ka BP (4 sites), 8.2–8.0 ka BP (3 sites), and 7.3–7.0 ka BP (1 site). The longest record of moraine deposition is from the Sisimiut-Kangerlussuaq region (a GrIS moraine sequence), which hosts moraines dated to ca. 11.6 ka BP, 10.3 ka BP, 9.2 ka BP, 8.2–8.0 ka BP, and 7.3–7.0 ka BP (Young et al., 2020a and references therein). As on Baffin Island, whereas no single site in Greenland hosts each pulse of moraine deposition, each dated moraine has an equivalent moraine at least at one other site. Considering all sites on Baffin Island and western Greenland, four intervals are identified where moraine deposition occurs on both sides of Baffin Bay: 11.8–11.6 ka BP, 10.4–10.2 ka BP, 9.2–9.0 ka BP, and 8.2–8.0 ka BP

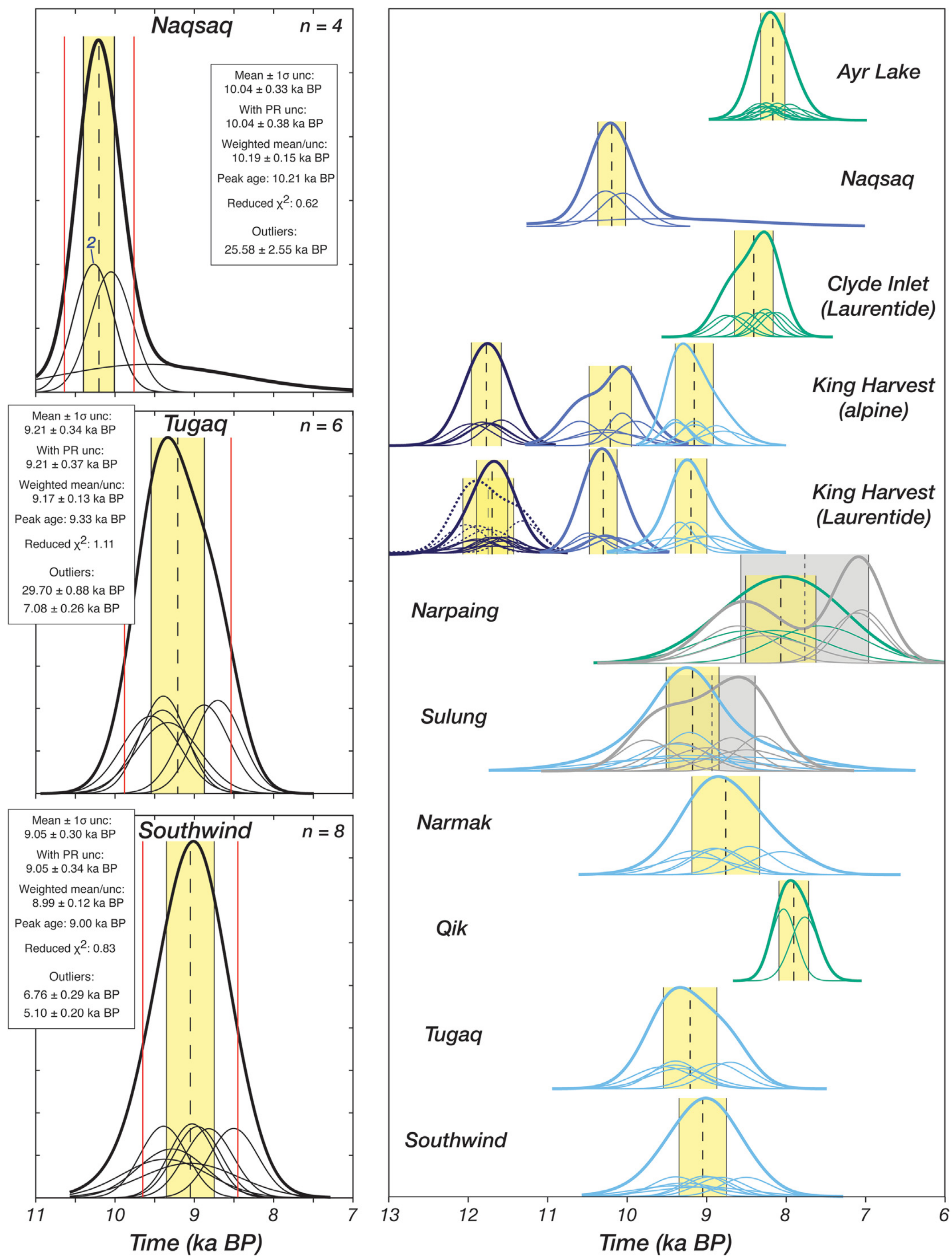

Fig. 6. Left panels – normal kernel density estimates for new ^{10}Be ages from moraine boulders. Three moraine boulder samples from Naqsaq valley (Fig. 1) were collected in CE 2013 and combined with a previous ^{10}Be age from the same moraine reported in Briner (2003); site description can be found in Young et al. (2015). Because of the low analytical resolution of this previous ^{10}Be age, we present a weighted mean as the most likely age of moraine deposition. Right panel – normal kernel density estimates for ^{10}Be-dated moraines across Baffin Island presented from north to south (see Fig. 1 for locations). Each estimate displays individual ^{10}Be ages (thin lines) and the summed distribution (thick line); yellow shading is the mean age ± 1 S.D. of the entire dataset. Ayr Lake (Young et al., 2012), Naqsaq (this study), Clyde Inlet (Briner et al., 2009b), King Harvest alpine and Laurentide (Young et al., 2020a). Datasets from Narpaing, Sulung, Narmak, Qik, and Tugaq are from Crump et al. (2020); the Sulung dataset includes 3 *in situ* ^{14}C ages (Crump et al., 2020; Young et al., 2014). At the Narpaing and Sulung sites, recessional moraines were also dated with ^{10}Be (grey). While morphostratigraphically younger, ^{10}Be ages are statistically indistinguishable from the primary moraine (color) and all ^{10}Be ages are combined as part of the stacked moraine record (Fig. 7). Note that Clyde Inlet is further constrained by independent bracketing ^{14}C ages of 7890 ± 150 and 8350 ± 150 and serves as a ^{10}Be production-rate calibration site (CURL-7038 and CURL-7046; Table 1; see Section 2.3). Unless otherwise noted, moraines at each site were deposited by alpine (non-Laurentide) ice; moraines attributed to Laurentide ice were deposited by fast-flowing outlet glaciers. Although cold-based ice is widespread across Baffin Island, especially at high elevations, warm-based erosive ice needed for moraine formation and cold-based ice is likely not a dominant feature at the sites hosting ^{10}Be-dated moraines depicted here.

Table 3
Baffin Island ^{10}Be sample information.

Sample	Latitude (N)	Longitude (W)	Elevation (m asl)	Thickness (cm)	Shielding	Quartz (g)[a]	Carrier added (g)[b]	^{10}Be/^{9}Be ratio[c]	±1σ Uncertainty	Blank-corrected ^{10}Be concentration (atoms g^{-1})[d]	Blank-corrected ^{10}Be conc. uncertainty (atoms g^{-1})	Age ka BP (Lm)	Age ka BP uncertainty	AMS Facility
Naqsaq														
13ELB-21	70.1466	70.2055	289	1.57	0.996	30.4154	0.1808	1.4252E-13	2.6790E-15	58,392	1414	10.27	0.25	LLNL-CAMS
13ELB-22	70.1462	70.1971	315	2.92	0.996	30.2120	0.1807	1.4398E-13	2.7069E-15	59,354	1437	10.27	0.25	LLNL-CAMS
13ELB-23	70.1466	70.1936	304	3.46	0.996	32.2151	0.1810	1.4736E-13	3.1701E-15	57,194	1503	10.05	0.27	LLNL-CAMS
CI11-01-1	70.1467	70.1893	263	2	0.996	27.37	0.51	1.2429E-13	7.1473E-15	154,763	15326	*25.58*	2.55	LLNL-CAMS
CI11-01-2	70.1463	70.1938	294	3	0.996	31.60	0.50	5.6534E-14	4.9483E-15	59,774	7113	9.57	1.14	LLNL-CAMS
												Weighted mean ± 1 S.D.	**10.19 ± 0.15 (0.24)**	
Boas Fiord - Tugaq														
Outboard erratics														
15BAC-01	66.7682	62.6741	219	1.98	0.997	25.8448	0.1988	1.2566E-13	3.3800E-15	66,704	2056	12.58	0.39	PRIME
15BAC-02	66.7706	62.6752	214	3.44	0.997	22.7741	0.2024	1.0499E-13	3.4900E-15	64,385	2350	12.35	0.45	PRIME
15BAC-03	66.7713	62.6777	191	2.80	0.997	26.3168	0.2029	1.1590E-13	3.4500E-15	61,664	2057	12.06	0.40	PRIME
												Mean ± 1 S.D.	**12.33 ± 0.26 (0.34)**	
Moraine boulders														
15BAC-04	66.7692	62.6819	169	1.23	0.996	42.7095	0.1996	1.1148E-13	3.6800E-15	35,955	1306	*7.08*	*0.26*	PRIME
15BAC-05	66.7659	62.2959	59	1.51	0.995	39.7403	0.2024	3.7383E-13	9.3800E-15	131,331	3855	*29.70*	*0.88*	PRIME
15BAC-06	66.7697	62.6829	160	1.83	0.996	24.2659	0.2000	7.6390E-14	2.6300E-15	43,431	1636	8.70	0.33	PRIME
15BAC-07	66.7717	62.6861	140	2.36	0.996	26.0760	0.2006	8.1300E-14	2.8900E-15	43,147	1669	8.87	0.34	PRIME
15BAC-08	66.7735	62.6903	130	2.36	0.992	29.5094	0.1996	9.6390E-14	3.4400E-15	44,988	1745	9.40	0.37	PRIME
15BAC-09	66.7598	62.2980	24	1.47	0.990	38.8572	0.2026	1.1393E-13	4.2400E-15	40,715	1661	9.54	0.39	PRIME
15BAC-10	66.7752	62.7098	68	3.06	0.996	41.9692	0.2004	1.2695E-13	3.8800E-15	41,839	1427	9.39	0.32	PRIME
15BAC-12	66.7752	62.7108	66	2.91	0.996	21.5669	0.1996	6.5080E-14	2.7400E-15	41,538	1862	9.33	0.42	PRIME
												Mean ± 1 S.D.	**9.21 ± 0.34 (0.37)**	
Southwind Fiord														
Outboard erratics														
15BRR-16	66.7545	62.3036	13	2.09	0.990	36.9631	0.2031	1.0390E-13	5.5300E-15	39,096	2184	9.32	0.52	PRIME
15BRR-18	66.7543	62.3052	5	1.66	0.990	36.6667	0.2031	1.0261E-13	4.5700E-15	38,917	1860	9.34	0.45	PRIME
Moraine boulders														
15BRR-01	66.7656	62.2851	145	1.69	0.998	21.4692	0.1994	6.5440E-14	2.3200E-15	41,916	1619	8.50	0.33	PRIME
15BRR-03	66.7658	62.2913	95	1.49	0.995	31.2701	0.2008	9.2640E-14	3.1800E-15	41,047	1541	8.82	0.33	PRIME
15BRR-04	66.7658	62.2928	89	3.27	0.994	35.4556	0.2018	1.0950E-13	3.3400E-15	42,699	1482	9.38	0.33	PRIME
15BRR-05	66.7659	62.2959	59	2.63	0.995	44.6652	0.1990	1.2897E-13	4.2300E-15	39,661	1432	8.96	0.32	PRIME
15BRR-06	66.7655	62.3036	37	3.38	0.997	42.6429	0.2000	1.1985E-13	3.7500E-15	38,796	1348	9.03	0.31	PRIME
15BRR-07	66.7566	62.2895	112	1.79	0.984	43.0966	0.2000	7.5030E-14	2.7400E-15	24,018	951	*5.10*	*0.20*	PRIME
15BRR-11	66.7569	62.2809	161	2.32	0.990	25.9095	0.2029	8.3750E-14	5.5100E-15	44,804	3076	9.05	0.62	PRIME
15BRR-12	66.7569	62.2827	146	3.25	0.990	25.1569	0.2027	8.2180E-14	4.6700E-15	45,224	2710	9.36	0.56	PRIME
15BRR-13	66.7567	62.2848	132	2.73	0.990	34.4471	0.2028	8.0570E-14	3.1100E-15	32,388	1378	*6.76*	*0.28*	PRIME
15BRR-15	66.7564	62.3009	27	2.19	0.990	39.8769	0.2033	1.1308E-13	5.1400E-15	39,512	1919	9.28	0.45	PRIME
												Mean ± 1 S.D.	**9.05 ± 0.30 (0.34)**	
Inboard erratics														
15BRR-08	66.7621	62.2987	16	3.08	0.990	26.7883	0.2003	7.2710E-14	2.8500E-15	37,500	1578	8.98	0.38	PRIME
15BRR-10	66.7584	62.3002	14	1.87	0.990	34.6426	0.2029	1.6108E-13	5.5000E-15	64,838	2444	*15.48*	*0.59*	PRIME

[a] Quartz and carrier weights for samples CI11-01-1 and CI11-01-2 were made on 2-digit balance.
[b] Samples were spiked with LDEO carriers 5.1 and 6 with evaporation-corrected ^{9}Be concentrations ranging from 1032.4 to 1035.5 ppm (see Table 4). Samples CI11-01-1 and CI11-01-2 were spiked with a 1000 ppm SPEX brand carrier.
[c] Samples were measured at either the Lawrence Livermore National Laboratory - Center for Accelerator Mass Spectrometry (LLNL-CAMS) or the Purdue Rare Isotope Measurement Laboratory (PRIME). Ratios are not corrected for ^{10}Be detected in procedural blanks, except for samples CI11-01-1 and CI11-01-2.

[d] Concentrations are blank corrected by subtracting the total number of ^{10}Be atoms in the process blank (Table 2); ratios for samples CI-01-1 and CI-01-2 are blank-corrected.
Ages are calculated using version 3 of the exposure age calculator found at https://hess.ess.washington.edu/(wrapper: 3.0, muons: 1 A, consts: 3.0.3), which implements an updated treatment of muon-based production (Balco et al., 2009; Balco, 2017). All ages are calculated using 'Lm' scaling and a Baffin Bay production rate of 4.04 ± 0.07 atoms g^{-1} yr^{-1} (Young et al., 2013a). This value has been updated from the CRONUS v2 value of 3.96 ± 0.07 atoms g^{-1} yr^{-1}; the calibration dataset is the same. All samples use a density of 2.65 g cm^{-3}, standard air pressure 'std', and an effective attenuation length of 160 g cm^{-2}.10Be concentrations are reported relative to 07KNSTD with a reported ratio of 2.85×10^{-12} using a ^{10}Be half-life of 1.36×10^{6} years.

(Fig. 6; Fig. 7). Moraines dated to ca. 9.7–9.6 ka BP (2 sites) and ca. 7.3 ka BP (Sisimiut-Kangerlussuaq) on western Greenland are the only intervals of moraine deposition not recorded on Baffin Island.

The site-to-site variability in the number of moraines hosted at individual locations throughout Baffin Bay is in part dictated by the nuances of moraine preservation. The moraine record at any individual site is inherently discontinuous as any moraine sitting on the landscape has the potential to be overrun and destroyed by a later advance of the ice margin (e.g., Gibbons et al., 1984; Young et al., 2011c). In the absence of cold-based ice, a moraine can only be preserved on the landscape if any subsequent advance of an ice margin is less extensive than the position of the previously deposited moraine. Sites that only host a moraine(s) correlative with a younger mode in Baffin Bay moraine deposition could in part be explained by this younger glacier advance overrunning and destroying older moraines. For example, the Ayr Lake site in north-central Baffin only hosts moraines dated to ~8.2 ka BP (Fig. 6), allowing for the possibility that moraines pre-dating 8.2 ka BP (e.g., the common 9.2–9.0 ka moraines) did exist, but glacier advance ca. 8.2 ka BP overran them. In contrast, the Naqsaq valley site only hosts moraines dated to ca. 10.2 ka BP (Fig. 6) and the last millennium (Young et al., 2015). Here, any 9.2 ka BP or 8.2 ka BP moraine that may have existed would have been overrun by glacial phases dating to the last millennium. Interestingly, the Ayr Lake and Naqsaq sites rest in neighboring valleys only ~25 km apart and differences in centennial-scale climate likely cannot explain the site-to-site differences in moraine preservation. If solely the Ayr Lake and Naqsaq valley ^{10}Be chronologies existed, one might invoke non-climatic dynamic factors or geomorphic factors (e.g., accumulation area, hypsometry) to explain the apparent asynchronicity in glacier behavior in neighboring valleys. When evaluated within the context of moraine deposition across Baffin Island or Baffin Bay, however, both valleys appear to record changes in regional climate, but with localized ice dynamical factors leading to glacier responses of varying proportion, and thus moraine preservation, but ice dynamical factors are not affecting the timing of moraine deposition.

Another factor that influences the number of moraines preserved at a single site is the location of the ice margin with respect to the ocean and the modern ice margin at any given time. At Jakobshavn Isbræ, the ice margin did not retreat out of Disko Bugt until ca. 10.2 ka BP and had retreated behind the modern margin by ca. 7.5 ka BP (Young et al., 2011a; Corbett et al., 2011). Thus, only moraines deposited between ca. 10.2–7.5 ka BP can be preserved on the modern landscape and, accordingly, only moraines dated to ca. 9.2 ka BP and 8.2 ka BP are found in the Jakobshavn Isbræ forefield. At 11.8–11.6 ka BP and 10.4–10.2 ka BP when moraines are being deposited at other Baffin Bay locations, the ice margin in the Jakobshavn Isbræ region still terminated offshore, whereas if a moraine was deposited ca. 7.3 ka BP, it has since been overrun by late Holocene re-expansion of the GrIS. In contrast, the GrIS margin in the Nuuk-KNS region was likely offshore until ca. 11.2–10.7 ka BP and had already retreated behind the modern margin by ca. 10.2 ka BP, offering a relatively narrow window for moraine preservation (Larsen et al., 2015; Young et al., 2021). The only moraine in the immediate KNS forefield was deposited at 10.24 ± 0.36 ka BP and any younger moraine that may have once existed would have been overrun by the late Holocene readvance of the GrIS (Young et al., 2021).

Despite the discontinuous nature of the moraine record at any single location, two sites on opposing sides of Baffin Bay host the most comprehensive records of glacier change in the region. The King Harvest site on the Cumberland Peninsula hosts moraines dated to ~11.8–11.6 ka BP, 10.4–10.2 ka BP, and 9.2 ka BP (Fig. 6). Notably, each of these modes of moraine deposition at King Harvest

Table 4
Process blank ^{10}Be data.

Sample ID	Carrier added (g)	Carrier concentration	^{10}Be/^{9}Be ratio ± 1σ (10^{-16})	^{10}Be atoms	Samples applied to (Table 3):
LDEO Carrier 5.1					
BLK_1_2013Nov04	0.1812	1032.4	1.770 ± 3.588	***2213*** ± ***4487***	13ELB-21, -22
BLK_1_2014Feb17	0.1805	1035.5	2.491 ± 0.832	***3111*** ± ***1039***	13ELB-23
LDEO Carrier 6					
BLK_2018Jan25	0.2027	1033.1	0.800 ± 0.800	***1120*** ± ***1120***	15BAC-01, -02, −03
BLK_2018Feb02	0.202	1033.5	1.100 ± 1.150	***1535*** ± ***2093***	15BAC-04, -06, −07, −08, −10, −12; 15BRR-01, -03, −05, −06, −07, −08
BLK_2018Mar09	0.2023	1034.8	10.040 ± 5.600	***14,553*** ± ***7836***	15BAC-*05, -09;* 15BRR-*04, -10, -11, -12, -13, -15, -16, -18*

All ^{10}Be concentrations are reported relative to 07KNSTD with a reported ratio of 2.85×10^{-12} using a ^{10}Be half-life of 1.36×10^{6} years (Nishiizumi et al., 2007).

record advances of both a glaciologically independent alpine glacier and LIS outlets. The repeated synchronous advances of these ice masses requires changes in regional climate as the driving mechanism behind glacier advance and subsequent moraine deposition (Young et al., 2020a). The only remaining mode of moraine deposition on Baffin Island not seen in the King Harvest record is at ca. 8.2–8.0 ka BP (Fig. 6). In southwestern Greenland, moraines deposited between the coast and the modern ice margin in the Sisimiut-Kangerlussuaq region are dated to ca. 11.6 ka BP, 10.4 ka BP, 9.2 ka BP, 8.2 ka BP, and 7.3 ka BP, which serves as both the longest moraine record in western Greenland and across Baffin Bay (Fig. 7). The Sisimiut-Kangerlussuaq region is the widest swath of ice-free terrain in western Greenland, likely facilitating the preservation of a >4 kyr record of ice-margin change that is not possible at other Baffin Bay locations where the ice margin either terminated in the ocean or had already retreated behind the eventual present-day ice margin position. For example, at 11.6 ka BP most of the southwestern GrIS margin still terminated off the modern coastline, and by ca. 8.0–7.5 ka BP, with few exceptions, nearly all the southwestern GrIS margin had retreated behind the modern ice margin (Carlson et al., 2014; Larsen et al., 2015; Young and Briner, 2015; Young et al., 2021). The similarity between the King Harvest and Sisimiut-Kangerlussuaq moraine records indicates that both sites are recording regional changes in climate through the early Holocene (Young et al., 2020a). We consider ^{10}Be-dated moraines at King Harvest and in the Sisimiut-Kangerlussuaq region as the principal moraine records that track changes in climate across Baffin Bay. Although the remaining sites across Baffin Bay with ^{10}Be-dated moraines only capture certain pieces of the primary King Harvest and Sisimiut-Kangerlussuaq records, moraines at these sites are no less climatically significant (Fig. 6; Fig. 7).

Statistically identical moraine ages, defined as overlapping mean ± S. D. moraine age from site to site, at 11.8–11.6 ka BP, 10.4–10.2 ka BP, 9.7–9.6 ka BP, 9.2–9.1 ka BP, 8.2–8.0 ka BP, and 7.3–7.0 ka BP indicate that regardless of ice-margin type and its response time to a climate perturbation, ice-margin changes are coeval within the resolution of our chronologies (Fig. 6; Fig. 7; Table S1); any asynchrony in ice-margin change cannot be detected with the ^{10}Be chronometer. We capitalize on this large dataset by merging ^{10}Be ages from each individual site at each interval of moraine deposition to best constrain the timing of synchronous advances of Baffin Bay ice masses and therefore regional climate perturbations across Baffin Bay (Fig. 7). Prior researchers have traditionally presented the mean ± S.D. of a^{10}Be population from moraine boulders as the best estimate for the timing of moraine deposition that accounts for all measurements, while not emphasizing any single sample that is part of a relatively small population size (e.g., Southwind and Boas fiord sites). To account for significantly larger ^{10}Be populations, we present the mean ± standard error of the mean (S.E.M.) for each mode in moraine deposition and propagate the uncertainty in the ^{10}Be production-rate calibration in quadrature. In doing so, we constrain regional culminations of glacier advance to 11.68 ± 0.22 ka BP (n = 23), 10.28 ± 0.19 ka BP (n = 40), 9.58 ± 0.19 ka BP (n = 18), 9.04 ± 0.17 ka BP (n = 65), 8.09 ± 0.15 ka BP (n = 52), and 7.24 ± 0.17 ka BP (n = 6; Fig. 7B; Table S2). We note that this composite glaciation curve only includes moraine boulders and does not include what are often closely limiting maximum or minimum constraining ^{10}Be ages from samples located immediately inboard or outboard of a directly dated moraine (Fig. 7).

5. Discussion

5.1. ^{10}Be dating in Baffin Bay

The regional efficacy of sub-glacial erosion and field sampling strategies are likely the primary factors driving the internal consistency in ^{10}Be ages at any individual site and across Baffin Bay. Southwestern Greenland appears particularly suitable for developing ^{10}Be-based records of GrIS and alpine glacier change. A 2016 survey revealed that only ~14% of all ^{10}Be measurements made in southwestern Greenland up to that point were influenced by isotopic inheritance as defined by the original authors (Young et al., 2016). This percentage decreases to ~6% when only considering low-elevation samples (<600 m asl), which is the typical elevation range for ^{10}Be measurements used to constrain Holocene fluctuations of the GrIS. As perhaps an extreme example of the overall lack of isotopic inheritance in southwestern Greenland is the landscape fronting Jakobshavn Isbræ, and across the broader Disko Bugt region, which is virtually inheritance free (Corbett et al., 2011; Young et al., 2011; Young et al., 2013a; Kelley et al., 2013, 2015). Epicenters of isotopic inheritance on southwestern Greenland are largely restricted to two environments. Inheritance is slightly more common at the highest elevations between Sisimiut and Kangerlussuaq (e.g., Rinterknecht et al., 2009; Roberts et al., 2009; Winsor et al., 2015), and inheritance also appears to be more prevalent in the KNS region (e.g., Larsen et al., 2015; Young et al., 2021, Fig. 1). High-elevation landscapes in the Sisimiut-Kangerlussuaq region are likely ice covered for shorter durations during glacial cycles and more susceptible to non-erosive cold-based ice cover than lower elevations. The KNS region is characterized by a dense fjord network likely promoting selective linear erosion (i.e., Sugden, 1978).

Southwestern Greenland is heavily influenced by the relatively warm West Greenland Current, whereas Baffin Island, despite occupying the same latitude range as southwestern Greenland, is characterized by a colder climate due to the Baffin Current transporting cold Arctic waters along the Baffin Island coast (Fig. 1). Compared to other polar locations, the relatively warm climate of southwestern Greenland likely helps facilitate the consistent

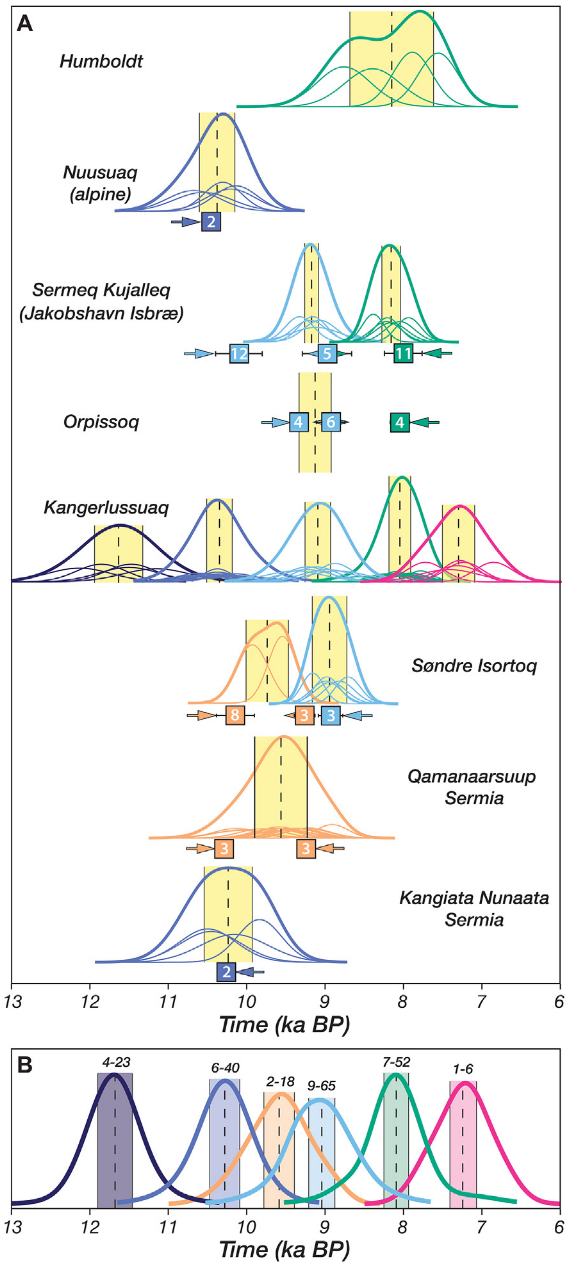

Fig. 7. (A) Normal kernel density estimates for ^{10}Be-dated moraines across western Greenland presented from north to south (see Fig. 1 for locations). Humboldt (Reusche et al., 2018), Nuusuaq (O'Hara et al., 2017), Sermeq Kujalleq (Young et al., 2011a, 2013a, 2013b; Corbett et al., 2011), Orpissoq (Young et al., 2013a), Kangerlussuaq (Winsor et al., 2015; Levy et al., 2018; Young et al., 2020a), Søndre Isortoq (Lesnek and Briner, 2018), Qamanaarsuup Sermia (Young et al., 2021), Kangiata Nunaata Sermia (Young et al., 2021). Boxes mark maximum-limiting (right pointing arrows) and minimum-limiting (left pointing arrows) ^{10}Be ages from erratic boulders or bedrock located immediately outboard or inboard of each target moraine. Maximum- and minimum-limiting constraints are shown as the average ^{10}Be age of each dataset (n = number within each box; see Table S1). For the Humboldt ^{10}Be age distribution, we excluded two older ^{10}Be ages of 11.35 ± 0.74 ka BP and 11.16 ± 0.71 ka BP that were originally included in a weighted-mean age estimate for this moraine (Table S1: Reusche et al., 2018). Subsequent work suggests these ages likely pre-date the timing of regional deglaciation (i.e., isotopic inheritance) and therefore we exclude them from the population (Ceperley et al., 2020). Young et al. (2020a) dated a moraine to ~8.6 ka BP that is stratigraphically bracketed by moraines dating to ca. 9.0 and 8.0 ka BP as part of the Kangerlussuaq moraine sequence. These ^{10}Be ages are not plotted, however, as this age assignment is based on only three ^{10}Be ages. Unless otherwise noted, moraines at each site were deposited by the GrIS; Humboldt, Sermeq Kujalleq, Qamanaarssup, and Kangiata Nunaata Sermia are outlet glaciers. (B) ^{10}Be ages from moraines on Baffin Island and western Greenland stacked to form a composite record of Baffin Bay moraine deposition; shading marks the mean ± standard error of the mean with the production-rate uncertainty propagated through in quadrature (Section 4; Table S2). Listed above each normal kernel density estimate is the number of field sites and ^{10}Be ages comprising each composite curve. Note that the composite curves only include moraine boulders and do not account for the minimum- and maximum-limiting ^{10}Be age from outboard and inboard of moraine segments.

presence of erosive warm-based ice (Young et al., 2016). The combination of widespread warm-based ice, lack of extensive fjord networks, and a landscape that rests well inboard of the GrIS margin during glacial maxima (i.e., longer durations of ice cover per glacial cycle), makes it more likely that any ^{10}Be accumulated on the landscape during previous ice-free periods is removed through subglacial erosion. The widespread occurrence of cold-based Laurentide ice, in part dictated by the influence of the Baffin Current on regional climate, and a landscape that rests comparatively closer to LIS margin during glacial maxima (i.e., shorter durations of ice cover per glacial cycle) contributes to a Baffin Island landscape where isotopic inheritance is more common (Young et al., 2016). Many ^{10}Be datasets that explicitly target the early to late Holocene histories of the LIS and alpine glaciers (versus LIS dynamics during the LGM), however, appear to be less influenced by inheritance (Crump et al., 2020; Young et al., 2012, 2015, 2020a; Table S1). Indeed, these datasets tend to be concentrated within fiords or at fiord heads (e.g., Briner et al., 2009a), or in alpine valleys (e.g., Young et al., 2020a) and largely avoid inter-fiord uplands or coastal lowlands where ice tends to be less erosive (Briner et al., 2006; Davis et al., 2006; Margreth et al., 2016).

Supplementing ^{10}Be ages directly from moraines with minimum- and maximum-limiting ^{10}Be ages from samples beyond and within targeted moraines has proven useful, particularly in southwestern Greenland where this approach has been widely applied (Fig. 7). While ^{10}Be ages from moraine boulders directly date the moraine itself, moraine boulders can be susceptible to exhumation, producing a ^{10}Be age that post-dates the true age of moraine deposition (e.g., Applegate et al., 2012; Crump et al., 2017), or suitable moraine boulders for sampling may not exist. ^{10}Be ages from moraine boulders in southwestern Greenland tend to display minimal scatter, yet in many instances dedicated efforts to sample boulders perched on bedrock or bedrock surfaces immediately inboard or outboard of a moraine help constrain the timing of moraine deposition (Young et al., 2013a). ^{10}Be ages in the Disko Bugt region best illustrate the relationship between ^{10}Be-dated moraines and limiting ^{10}Be ages. At Jakobshavn Isbræ ^{10}Be ages from the Tasiussaq moraine and from bedrock and erratic boulders located immediately inboard of the moraine are statistically identical (Corbett et al., 2011; Young et al., 2011a, 2011b, Fig. 7). In this case, either of these two datasets can be used to constrain the age of the Tasiussaq moraine, but erratic boulders perched on bedrock located immediately inside a moraine are not susceptible to landscape degradation that can affect moraine boulders. In the southern Disko Bugt region at Orpissoq, both the Marrait and Tasiussaq moraines are preserved on the landscape, but neither hosts boulders suitable for ^{10}Be sampling. Yet, ^{10}Be ages from boulders perched on bedrock outboard and inboard of Marrait moraine provide close bracketing ages on the moraine itself, and ^{10}Be ages from immediately inside the Tasiussaq moraine constrain moraine deposition to ~8.2 ka BP (Fig. 7). ^{10}Be ages from outboard of moraine provide maximum-limiting ^{10}Be ages on a moraine, but these ^{10}Be ages need not be close maximum-limiting ages if moraine deposition was the result of a significant ice-margin re-advance (Young et al., 2013a). ^{10}Be ages from erratic boulders perched on bedrock immediately inboard of a moraine, however, should always provide a close-minimum constraining age for the moraine, or should be statistically identical to the moraine age derived from moraine boulders (Fig. 7).

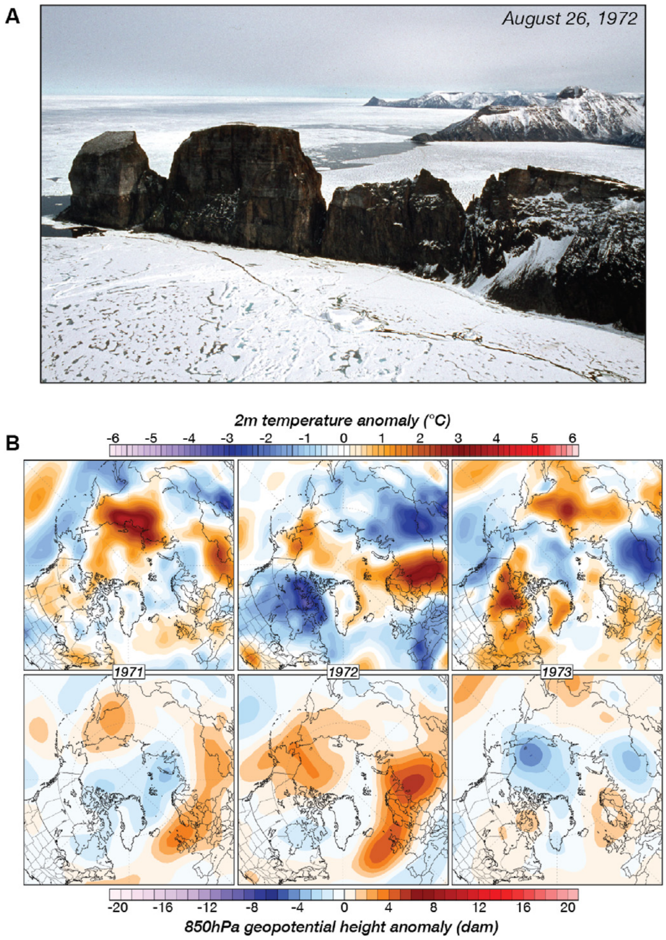

Fig. 8. (A) Photograph taken on August 26th, 1972, looking to the southeast across Qaqulluit and a sea-ice-covered southern Baffin Bay (see Fig. 2A; Photo credit: G. Miller). Sea ice along Baffin Island typically breaks up by early July followed by ice-free conditions through the remainder of the summer and into early autumn. In 1972, sea ice from the previous winter never broke up during the summer. (B) Top row – summer (JAS) temperature anomalies at 2 m for 1972 (center) compared to the preceding (1971) and following (1973) years; the Baffin Island region is characterized by a temperature anomaly of ~4–7 °C in 1972. Bottom row – 850 hPa geopotential height anomaly over the same period. Anomalies are relative to the 1960–1990 average using the NCEP/NCAR reanalysis version 1 dataset (U. Maine Climate Reanalyzer, www.cci-reanalyzer.org). Figure is not meant to suggest that expanded sea ice in 1972 is a result of a freshwater anomaly, only that expanded sea ice in the summer season can contribute to summer cooling.

5.2. Early holocene freshwater discharge, regional cooling, and glacier advance in Baffin Bay

The synchronous behavior of the GrIS, LIS, and alpine glaciers is most readily explained by changes in temperature because it is unlikely that synchronous changes in winter precipitation would occur across such a large area (i.e., Ten Brink and Weidick, 1974; Young et al., 2020a). The most compelling evidence that synchronous advances of Baffin Bay ice masses were driven by changes in temperature, however, is the coherency between ^{10}Be-dated moraines, freshwater outburst events, and early Holocene temperatures recorded in Greenland ice. The 8.2 ka cooling event is the most well-known abrupt climate perturbation of the Holocene and is thought to have been driven by the sudden drainage of ice-dammed lakes at the southern margin of the LIS, with perhaps contributions from the collapse of the Hudson Bay ice saddle, into the Labrador Sea (Alley et al., 1997; Alley and Ágústsdóttir, 2005; Barber et al., 1999; Wagner et al., 2013; Matero et al., 2017; Gauthier et al., 2020). Similar to the 8.2 ka cooling event, the 9.3 ka cooling event has also been interpreted to be driven by the release of freshwater into the North Atlantic (Yu et al., 2010; Jennings et al., 2015). Although uncertainties remain surrounding the exact magnitude of freshwater release for both the 8.2 ka and 9.3 ka cooling events (e.g., Aguiar et al., 2021), these events are clearly recorded in Greenland ice and, arguably, provide the most unambiguous relationship between the input of freshwater into the western North Atlantic region, its effect on Atlantic meridional overturning circulation (AMOC), and regional-to hemispheric-scale cooling (Alley and Ágústsdóttir, 2005). With a well-established sequence of events – freshwater release into the Labrador Sea region, AMOC reduction and likely sea-ice expansion, and regional cooling – the 8.2 ka and 9.3 ka cooling events provide a consistent framework in which to 1) gauge the sensitivity of Baffin Bay ice masses to known abrupt climate change, and 2) assess the potential drivers of glacier advance in the Baffin Bay region that are not associated with the 8.2 ka or 9.3 ka cooling events.

The 9.3 ka event is characterized by 2–3 °C mean-annual cooling over ~100 years, whereas the ~160-year-long 8.2 ka event is characterized by 3–4 °C of mean-annual cooling based on gas-phase temperatures from Greenland ice (Kobashi et al., 2007, 2017). Moraines in the Baffin Bay region deposited by the LIS, GrIS and alpine glaciers at ca. 9.2–9.0 and 8.2–8.0 ka BP provide evidence that both cooling events were of sufficient magnitude and duration to elicit responses from Baffin Bay ice masses. While perhaps unsurprising that Baffin Bay glaciers advanced in response to regional cooling, the subtleties of the moraine and gas-phase temperature records provide additional details on the nature of regional cooling during the 9.3 and 8.2 ka BP cooling events and the processes that allow glaciers and ice sheets to respond to this cooling. Gas-phase temperature reconstructions from Greenland ice reflect mean annual temperatures which, in turn, are likely biased towards winter temperatures, in particular during episodes of abrupt climate change in the North Atlantic region (Buizert et al., 2014). This wintertime bias is driven by the rapid expansion of winter sea ice during periods of freshwater induced AMOC reduction, resulting in exceptionally cold winters (i.e., seasonality hypothesis; Denton et al., 2005). The response of Baffin Bay ice masses to the 8.2 ka and 9.3 ka events, however, requires that these cooling events included some degree of summertime cooling as the position of glacier and ice-sheet margins is dictated by summer temperature. Increased wintertime precipitation also drives fluctuations in ice-margin position, but snowfall in glacier and ice sheet accumulation zones must be propagated down-ice to the terminus, which, for ice sheets, takes several centuries to millennia (e.g., Lowell et al., 1999). The combination of temperature reconstructions from Greenland ice and the Baffin Bay moraine record reveals that the freshwater-forced 8.2 ka and 9.3 ka abrupt cooling events, which are characterized by reduced AMOC and expanded winter sea ice, included a component of summertime cooling despite being primarily wintertime phenomena (Fig. 8; Fig. 9).

Regional cooling centered at ca. 10.5–10.4 ka BP in Greenland ice cores, combined with a distinct pulse in moraine deposition across Baffin Bay at this time, shares the same characteristics as the 8.2 and 9.3 ka cooling events which are also characterized by regional cooling and a distinct pulse in moraine deposition (Fig. 9; Kobashi et al., 2017). Moreover, the link between freshwater input into the Labrador Sea region, AMOC reduction, and attendant cooling at ca. 10.5–10.4 ka BP is supported by a record of iceberg discharge through Hudson Strait which provides compelling evidence for the consistent freshwater forcing of cold climate events during the early Holocene (Fig. 9; Jennings et al., 2015). O'Hara et al. (2017) proposed a connection between the record from Jennings et al.

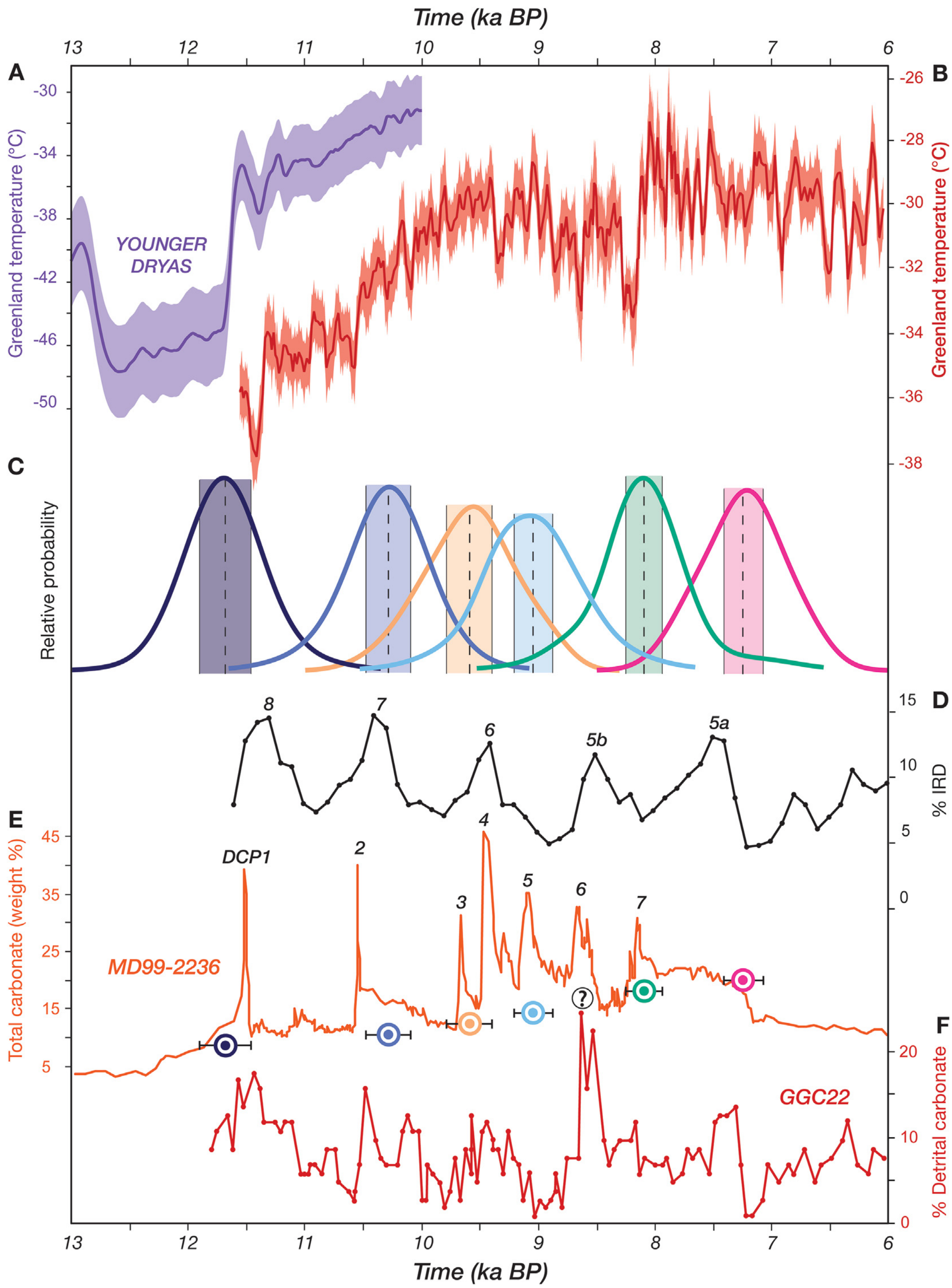

Fig. 9. (A) Greenland mean-annual temperatures reconstructed using gas-phase $\delta^{15}N-N_2$ measurements (purple; $\pm1\sigma$; Buizert et al., 2014). (B) Greenland mean-annual temperatures reconstructed using gas-phase $\delta Ar-N_2$ measurements (red; $\pm2\sigma$; Kobashi et al., 2017). (C) Baffin Bay moraine stack from Fig. 7B; shading is the mean moraine age ±1 S.E.M. including the ^{10}Be production-rate uncertainty. (D) Ice-rafted detritus stack from Bond et al. (2001). This stack comprises 4 records including GGC22 in panel F. Numbers mark previously identified Bond events. (E) Carbonate weight percentage from core MD99-2236 positioned on the Cartwright Saddle (Jennings et al., 2015). DCP - detrital carbonate peak. (F) Detrital carbonate percentage from core GGC22 located southeast of Newfoundland (Bond et al., 2001). To help orient the reader, bullseyes on panel E mark the mean age ±1 S.E.M. including the ^{10}Be production-rate uncertainty of each moraine from panel C and Fig. 7B. The tentative datapoint at 8.6 ka BP is a ^{10}Be-dated moraine reported in Young et al. (2020a) and Briner et al. (2020) based on only 3 ^{10}Be ages.

(2015) and GrIS and Greenland mountain glacier phases, and this was later expanded upon with a much larger dataset by Young et al. (2020a). Seven peaks in detrital carbonate (DCP) deposition between ca. 11.5–8.0 ka BP are interpreted to reflect the episodic release of icebergs and freshwater into the Labrador Sea (Jennings et al., 2015, Fig. 8). DCP7 and DCP4 are thought to mark freshwater release associated with 8.2 ka and 9.3 ka events (Jennings et al., 2015). DCP2 is centered at 10.5 ka BP and provides a plausible link to brief cooling seen in Greenland ice cores and coeval moraine deposition across Baffin Bay (Fig. 9). In this regard, freshwater discharge through the Hudson Strait, brief regional cooling, and moraine deposition ca. 10.5–10.4 ka BP shares the same characteristics as the 8.2 ka and 9.3 ka cooling events.

The link between freshwater input into the Labrador Sea region, AMOC reduction, and attendant cooling near the YD termination is likely not as straightforward as for the 8.2 and 9.3 ka events and cooling centered ca. 10.5–10.4 ka BP. DCP1 is centered at 11.6 ka BP and is correlative with a pulse of moraine deposition in Baffin Bay (Fig. 9), but it is unclear which episode of cooling is linked to this episode of freshwater discharge and moraine deposition. DCP1 occurs at the YD termination and it is tempting to link this episode of freshwater discharge to end-of-YD warming and Baffin Bay moraine deposition at the culmination of the YD. Freshwater-triggered cooling, however, requires that freshwater injection precedes both the cooling event and the episode of moraine deposition. Therefore, it is unlikely that the pulse of moraine deposition ca. 11.6 ka BP in Baffin Bay is linked to the 1200-yr-long YD cooling event. A second possibility is that DCP1 is the trigger for the Preboreal oscillation (PBO) at ca. 11.4 ka BP (Fig. 9; Kobashi et al., 2017) and subsequent moraine deposition in Baffin Bay. This scenario would satisfy the requirement that a freshwater injection event precedes the cooling event, but the timing of moraine deposition (11.68 $\pm$ 0.22 ka BP) appears to pre-date the PBO (Fig. 9). Although the uncertainties in the timing of moraine deposition overlap with the PBO, ^{10}Be ages across Baffin Bay at 10.5–10.4 ka BP, 9.3 ka BP, and 8.2 ka BP are tied more closely with a cooling event, sometimes slightly post-dating a cooling event, which is consistent with the phasing needed to relate regional cooling and moraine deposition (Fig. 9). A third possibility is that DCP1 marks an episode of freshwater discharge within the late YD that triggered a brief cooling event at the YD termination, which in turn led to brief readvances of Baffin Bay glaciers. It is unlikely that the age of DCP1 can be shifted to the beginning of the YD, and thus DCP1 is almost certainly not the YD triggering mechanism. We cannot yet determine if DCP1 and moraine deposition across Baffin Bay is related to the PBO or a brief episode of cooling around the YD termination. Yet, remaining ^{10}Be ages in the region consistently fall within or slightly post-date cooling centered at ca. 10.5, 9.3, and 8.2 ka BP (Fig. 9), whereas ^{10}Be ages of 11.8–11.6 ka BP consistently pre-date the PBO. We suspect that moraine deposition in Baffin Bay near the YD termination does not relate to the PBO, although we acknowledge that a link between the Jennings et al. (2015) LIS detrital carbonate record, the Baffin Bay moraine record, and the PBO would be consistent with the phasing of later events centered at 10.5, 9.3, and 8.2 ka BP.

Advances of the GrIS at ca. 9.7–9.6 ka BP and 7.3–7.0 ka BP are more difficult to characterize. DCP3 is centered at 9.7 ka BP, which, again, provides a plausible and consistent link between freshwater discharge through Hudson Strait and an advance of the GrIS. Unlike cooling centered ca. 10.5 ka BP, 9.3 ka BP, and 8.2 ka BP, however, no distinct cooling episode ca. 9.7 ka BP is recorded in Greenland ice cores (Fig. 9). Moraine deposition ca. 7.3–7.0 ka BP (Ørkendalen) is perhaps linked to centennial-scale cooling is observed in Greenland ice cores ca. 7.4–7.2 ka BP (Fig. 9). There is not a well-defined peak in carbonate deposition at this time, but the overall level of carbonate deposition between ca. 8–7 ka BP is above the baseline carbonate values that are recorded prior to ca. 12 ka BP and after 7 ka BP (Fig. 8), suggestive of enhanced iceberg and freshwater delivery during at this time. We also note that unlike the older moraine systems in the Kangerlussuaq region that are more isolated and clearly defined, the Ørkendalen ice limit is a broad moraine system characterized by hundreds of undifferentiated moraine crests. This distinct morphology suggestive of a stagnating ice margin (versus an ice-margin readvance) could perhaps represent the response of the GrIS to a more low-amplitude, rather than abrupt, episode of cooling.

The clearest relationship between an episode of moraine deposition and pulses of freshwater input occurs ca. 10.5–10.4 ka BP, 9.3 ka BP, and 8.2 ka BP, likely corresponding to DCP 2, DCP 4, and DCP 7 (Fig. 9; Jennings et al., 2015; Young et al., 2020a). Additional pulses in moraine deposition ca. 11.6 ka BP and 9.7–9.6 ka BP are perhaps linked to DCP 1 and DCP 3 (Fig. 9). Of the well-defined DCPs sourced from the Hudson Strait, DCP 5 and DCP 6 do not have an obvious pairing within the Baffin Bay moraine record. Whereas the timing of DCP 5 overlaps with a pulse of moraine deposition linked to the 9.3 ka BP event, DCP 4 slightly precedes moraine deposition and is thus a better candidate as the 9.3 ka BP event trigger (Jennings et al., 2015). DCP 6 does not appear to be reflected in the moraine record, however, a recessional moraine in the Kangerlussuaq region of southwestern Greenland dates to ca. 8.6 ka BP, but this age is based on only 3 ^{10}Be ages and has not been reproduced at any other location; it remains unknown of there was widespread glacier advance and/or stillstand at this time in the Baffin Bay region (Fig. 9; Young et al., 2020a; Briner et al., 2020). Nonetheless, there exists a striking similarity between the Baffin Bay composite moraine record and the record of detrital carbonate peaks (freshwater) sourced from Hudson Strait. Because the moraine record is inherently discontinuous (see Section 4), it is perhaps not surprising that each DCP is not reflected in the moraine record; one possibility is that moraines correlating to DCP 5 may have once existed on the landscape but were overrun by readvances triggered by DCPs 6 and 7, or these moraines do indeed exist, but have yet to be identified and well dated.

The 8.2 ka event provides a known template for the relationship between freshwater input into the Labrador Sea via the Hudson Strait, regional cooling, and glacier response. Although the exact timing of this sequence of events at each of our identified phases of moraine deposition is difficult to pinpoint when considering the inherent chronological uncertainties in each proxy, treating these intervals as near-duplicates of the 8.2 ka event serves a consistent mechanistic framework to explain the origins of early Holocene cooling events and the attendant response of the cryosphere. Critical to this framework is the likely involvement of expanded sea ice cover enhancing abrupt cooling. Expanded sea ice magnifies wintertime temperature depressions (i.e., Denton et al., 2005), but we hypothesize that summertime temperatures are also susceptible to the effects of winter sea ice because changes in summer temperature are needed to drive synchronous changes in Baffin Bay glacier change. One possible mechanism allowing expanded winter sea ice to influence summer temperatures is a reduction in the length of the summer ablation season. Expanded and/or thicker winter sea ice would either take longer to break up in the following spring and early summer or would develop earlier in autumn preceding a year of extreme winter sea ice; either scenario would shorten the cumulative summer ablation season (Fig. 8). As glaciers' mass balance is sensitive to the cumulative effects of the summer ablation season, lingering summer sea ice is one mechanism that could reduce overall summer glacier melt needed to facilitate glacier re-advances in response to freshwater-forced abrupt cooling events.

5.3. The Baffin Bay moraine record and Bond events

Bond events are defined by ocean sediment layers with elevated levels of ice-rafted grains that have classically been interpreted as reorganizations of North Atlantic Ocean surface hydrography and climate during the Holocene (Bond et al., 2001). Considered a canonical record of Holocene climate variability, Bond events were originally attributed to variations in solar output with a cyclicity of ~1500 years. Several alternative forcing mechanisms have been proposed, but no single unifying theory on the origins of Bond events has been established (Wanner et al., 2011 and references therein). Contributing to the uncertainty surrounding the origins of Bond events has been difficulty in reproducing Bond events in marine archives (e.g., Alonso-Garcia et al., 2017; Bradley and Bakke, 2019; Zielhofer et al., 2019) while at the same time, Bond-like events do seem to appear in certain terrestrial archives of climate variability (e.g., Hu et al., 2003; Wang et al., 2005; Balascio et al., 2015; Cheng et al., 2015). Our newly created record of Baffin Bay glacier advances, coupled with arguably the most direct and well-resolved record of early Holocene iceberg and freshwater production via the Hudson Strait (Jennings et al., 2015), warrants a new assessment of the possible origins of early Holocene Bond events.

We speculate that Bond events in the early Holocene are the product of Hudson Strait discharge events defined by the Cartwright Saddle and GGC22 records of carbonate deposition (Fig. 9). In this scenario, carbonate-bearing icebergs and freshwater released through Hudson Strait follow the Labrador Current first over the MD99-2236 core site on the Cartwright Saddle followed by the GGC22 site, which was included in the original petrologic stack used to identify Bond events (Fig. 1). Freshwater becomes entrained in the North Atlantic current and subpolar gyre, which drives brief AMOC reduction, sea-ice expansion, regional cooling, and subsequent short-lived readvances advances of the LIS, GrIS, and alpine glaciers in the Baffin Bay region. Spikes in eastern Atlantic petrologic tracers do track the southward and eastern advection of cooler Labrador and Nordic surface waters as originally proposed (Bond et al., 2001). In this scenario, advection is likely not driven by low amplitude variations in solar output, but instead facilitated by the expansion of winter sea ice accompanying each freshwater-driven cooling event. Freshwater-driven abrupt cooling events in the early Holocene and the last glacial cycle almost certainly included the expansion of sea ice in the North Atlantic region, which in turn forced cooling recorded in Greenland ice cores (Alley and Ágústsdóttir, 2005; Denton et al., 2005; LeGrande and Schmidt, 2008; Morrill et al., 2013; Buizert et al., 2014; Li and Born, 2019). Expanded sea ice in the North Atlantic would result in lower regional temperatures, but a more southerly sea-ice extent would also drive the southward movement of the polar front as was thought to have occurred during Dansgaard-Oeschger events of the last glacial period (i.e., Barker et al., 2015). The southward shift of the polar front via sea-ice expansion is a plausible mechanism that would result in the southward and eastern advection of Labrador and Nordic surface waters needed to produce the record of petrologic tracers from the eastern North Atlantic that define Bond events.

Bond events were initially identified based on petrologic tracers sourced from Iceland, Jan Mayen, and eastern Greenland found in eastern North Atlantic sediments, and carbonate deposition off Newfoundland. Because of their similarity spanning opposite sides of the North Atlantic, these records were stacked to serve as an overarching proxy for the southward advection of cooler IRD-laden Nordic and Labrador Sea surface waters (Fig. 1; Fig. 9; Bond et al., 2001). In the original description of Holocene Bond events, it was noted that either event 5a or 5b was likely linked to the newly discovered 8.2 ka cooling event (Alley et al., 1997; Bond et al., 1997). Although changes in thermohaline circulation were suspected as playing a role in the 8.2 ka event at the time (Alley et al., 1997), the exact 8.2 ka triggering mechanism had yet to be identified. Following the identification of the suspected 8.2 ka event outburst flood (Barber et al., 1999), subsequent discussion of Holocene Bond events no longer correlated event 5 (a or b) to the 8.2 ka cooling event (Bond et al., 2001). Rather, Bond events were attributed to a ~1500-yr cycle in solar variability, including events 5a and 5b, one of which was previously associated with the 8.2 ka event. The hypothesis that changes in surface-ocean hydrography are triggered by subtle and quasi-periodic variations in solar output is difficult to reconcile with freshwater-forced cooling events in the North Atlantic region. The 8.2 ka event is the product of the random intersection of a retreating LIS margin, proglacial topography favoring the creation of a large ice-dammed lake, and a drainage outlet adjacent to a region where perturbations to ocean circulation can drive large-scale climate variability. Assuming the 8.2 ka event was indeed triggered by the drainage of ice-dammed lakes (i.e., Barber et al., 1999; Roy et al., 2011; Jennings et al., 2015), the exact timing of this event is inconsequential. The ~1500-yr cycle of Bond events through the Holocene is calculated from the timing of only 8 events through the Holocene (Bond et al., 2001); by not including one of these events because it is the product of a random freshwater discharge event controlled largely by topography would result in an apparent periodicity of something other than 1500 years. Another possibility is that the 8.2 ka event was a randomly timed occurrence that coincided with a solar-driven Bond event that was bound to occur approximately every 1500 years. It is conceivable that the timing of a single freshwater-forced cooling event driven by the sudden drainage of a proglacial lake and a Bond event is a coincidence, but the synchronous occurrence of 2 or more suspected freshwater-driven cooling events and Bond events seems unlikely.

Included in the original Bond petrologic tracer stack, and perhaps most relevant here, is the record of carbonate deposition off the Newfoundland coast (GGC22; Fig. 1; Fig. 9). This record was partly interpreted to reflect drift ice sourced from Baffin Bay and delivered to the core site via the Baffin and Labrador Currents (Bond et al., 2001). The location of GGC22, however, also occurs down current of the Cartwright Saddle and the mouth of Hudson Strait (Jennings et al., 2015). Any Hudson Strait discharge events should carry carbonate-bearing icebergs first over the Cartwright Saddle followed by across the GGC22 coring location via a branch of the Labrador Current (Reverdin et al., 2003; Fratantoni and McCartney, 2010; Condron and Winsor, 2011; Lewis et al., 2012; Jennings et al., 2015). The original interpretation of the GGC22 record as a proxy for drift-ice flux sourced from Baffin Bay and the southwards migration of colder surface waters allows for a consistent interpretation of carbonate flux through the entire Holocene. Yet, this approach makes no distinction between early Holocene discharge events sourced from the Hudson Strait and subsequent carbonate deposition in the middle to late Holocene, which likely cannot be sourced from the Hudson Strait due to there no longer being an ice source there. At the time of the original identification of Bond events, it had long been suspected that extreme iceberg and freshwater discharge events sourced from eastern Canada and the Hudson Strait had occurred repeatedly during the last glacial period (e.g., Broecker et al., 1992; Bond et al., 1992; Bond and Lotti, 1995), but this concept had yet to be established for the early Holocene.

Peaks in carbonate deposition on the Cartwright Saddle are strikingly similar to the record of carbonate deposition southwest of Newfoundland (GGC22), suggesting that both records track discharge events through the Hudson Strait (Fig. 1; Fig. 9). In turn, the Cartwright Saddle carbonate record is similar to the record of Bond events as identified by the trans-Atlantic marine stack (Fig. 9). Linking Bond events and freshwater-forced cooling events, however, is further complicated when considering the exact source of each pulse of carbonate deposition recorded on the Cartwright Saddle. Jennings et al. (2015) reasoned that a variety of mechanisms could result in the delivery of freshwater and detrital carbonate through Hudson Strait. Based on independent radiocarbon constraints, Jennings et al. (2015) attributed 7 primary peaks in detrital carbonate to a variety of plausible mechanisms: 1) an increase of iceberg production associated with an ice stream advance, 2) an increase of iceberg production associated with the break-up of an ice stream, 3) sudden drainage events (e.g., 8.2 ka event), and 4) waterway openings during the final phase of LIS deglaciation (e.g., Tyrell Sea). Whereas the initial mechanism of freshwater delivery may vary, the result is the same once freshwater enters the Labrador Sea region. To explicitly link Bond events to pulses of detrital carbonate and their suspected solar origins would require a mechanism that is able to drive glacier advance and retreat, trigger topographically controlled discharge events, and pace the final openings of waterways as the LIS retreated. Attributing peaks in detrital carbonate to low amplitude solar variability would perhaps be easier if each episode of carbonate deposition were the result of the same process (e.g., ice stream advance or retreat). Yet, the overall variety of freshwater delivery mechanisms, with particular emphasis on the seemingly random interplay between a retreating ice margin and topography required to facilitate the sudden drainages of proglacial lakes, makes it unlikely that distinct pulses of detrital carbonate through the Hudson Strait are manifestations of a solar-driven process.

Alternatively, the record of carbonate deposition on the Cartwright Saddle (and at the GGC22 site) does not reflect IRD and meltwater sourced from the Hudson Strait. Instead, IRD is from a more northerly carbonate source, perhaps consistent with the original description of carbonate sources and their link to surface ocean hydrography proposed by Bond et al. (2001). The Cartwright Saddle carbonate record, however, is dominated by calcite with relatively low abundances of dolomite consistent with the relative percentages of these minerals found in the Paleozoic carbonate bedrock flooring Hudson Strait (Andrews and Tedesco, 1992; Andrews et al., 1999; Hillaire-Marcel et al., 2007; Rashid et al., 2011). IRD sourced from more northerly Baffin Bay ice streams would likely contain high percentages of dolomite (Andrews et al., 2012; Jennings et al., 2015).

Freshwater discharge through Hudson Strait as a trigger for AMOC reduction, sea-ice expansion, regional cooling, glacier advance in Baffin Bay, and southwards migration of the polar front provides a consistent mechanism to explain early Holocene Bond events 8 through 5. The caveat of this hypothesis is that freshwater discharge through Hudson Strait cannot explain Bond events 4 through 1 occurring in the middle and late Holocene. Retreat of the LIS out of the Foxe Basin by ~7.1 ka BP would shut off the final supply of icebergs through Hudson Strait, which is supported by a significant drop in detrital carbonate deposition at this time on the Cartwright Saddle (Fig. 9; Dyke, 2004; Jennings et al., 2015). LIS-sourced meltwater from beyond Hudson Strait could have acted as a triggering mechanism for middle Holocene Bond events via river discharge, but the LIS had retreated out of Baffin Island fiords by ~8 ka BP (Dyke, 2004; Briner et al., 2009a, 2009b), thus likely removing the primary source for carbonate IRD, which in turn is needed to identify Bond events in marine sediments. Retreat of the southwestern GrIS margin through the early and middle Holocene (e.g., Young and Briner, 2015; Larsen et al., 2015; Lesnek et al., 2020; Young et al., 2021) could have acted as a freshwater source, but peaks in carbonate deposition off Newfoundland through the late Holocene point to increased drift-ice flux from the Canadian sector of Baffin Bay that must have accompanied any potential GrIS-meltwater forcing. Solely a western GrIS freshwater source would likely not yield episodes of increased carbonate deposition because western Greenland is composed almost entirely of crystalline bedrock with only minor carbonate outcrops in northern Greenland adjacent to the Nares Strait. It is possible that a combination of GrIS meltwater and alpine glacier melt from the Canadian sector of Baffin Bay could serve as a freshwater trigger for mid-to late Holocene Bond events, but this scenario would suggest AMOC sensitivity to freshwater fluxes that are likely much smaller than the large freshwater outburst events thought to be needed to significantly perturb AMOC (e.g., Morrill et al., 2013; Wagner et al., 2013). Nonetheless, Bond events in the late Holocene are thought to involve perhaps small changes in AMOC strength (e.g., Lund et al., 2006), and it remains plausible that Bond events in the Holocene were the result of several triggering mechanisms (Wanner and Bütikofer, 2008; Wanner et al., 2011).

A variety of hypotheses have been invoked to explain the origins of Bond events and no single hypothesis appears to be able to explain the occurrence of Bond events through the entire Holocene (Wanner et al., 2011). Moreover, it remains unclear if Bond events follow a solar-driven ~1500-yr cycle as originally proposed, or if this ~1500-yr cycle relates more so to oceanic circulation, or if Bond events instead are the product of several competing periodicities that are each reflected in North Atlantic marine archives (Debret et al., 2007). Because of the difficulty in attributing the low-amplitude solar variability to widespread changes in North Atlantic climate, it has long been suggested that changes in climate must have involved changes in ocean circulation (McManus et al., 1999; Broecker et al., 2001). Attributing early Holocene Bond events to repeated freshwater discharge through the Hudson Strait provides a hypothesis that bypasses any solar-related triggering mechanism while emphasizing the likely important role of ocean circulation driving early Holocene climate variability in the North Atlantic region.

6. Conclusions

Prominent moraine systems on western Greenland and Baffin Island have been of interest to glacial geologists and paleoclimatologists for over half a century. Early researchers proposed that widespread moraines on opposing sides of Baffin Bay were equivalent features and climatic in origin. Decades of traditional radiocarbon constraints, however, supported a scenario where moraine deposition did not occur synchronously across Baffin Bay and could not be attributed to widescale changes in regional climate. The prevailing view of asynchronous moraine deposition, and therefore non-climatic in origin, remained largely unchanged for decades, but traditional radiocarbon ages did constrain a relatively narrow window of time in which moraine deposition could occur. Over 10+ years of focused ^{10}Be-based chronologies in the Baffin Bay region have produced a detailed picture of LIS, GrIS, and alpine glacier change that is consistent with the broad timing of moraine deposition provided by decades of radiocarbon constraints. ^{10}Be ages have identified pulses of moraine deposition at ca. 11.8–11.6 ka BP, 10.4–10.2 ka BP, 9.3 ka BP, and 8.2 ka BP, with perhaps additional moraine deposition occurring ca. 9.7 ka and 7.3 ka. Because these modes encompass moraines deposited by the LIS, GrIS, and independent alpine glaciers, moraine deposition is likely the result of widespread changes in regional climate at these times. Moreover, pulses of moraine deposition in Baffin Bay are likely correlative with ^{10}Be-dated moraines deposited by the Labrador sector of the LIS further supporting changes in regional climate drove widespread synchronous glacier advances (i.e., Ullman et al., 2016). Early researchers were incorrect in surmising that moraines distributed on Baffin Island and western Greenland were the product of a single climate event, yet they were likely correct in that moraines are indeed equivalent features, but instead are the product of several climatic events.

The timing of moraine deposition across Baffin Bay coincides with repeated pulses of IRD and meltwater via the Hudson Strait in the early Holocene, including during the 8.2 ka BP event (i.e., Jennings et al., 2015). The relatively well-constrained dynamics of the 8.2 ka BP event provide a template for assessing Baffin Bay ice-margin behavior. Freshwater discharge through the Hudson Strait associated with the 8.2 ka cooling event triggered brief AMOC reduction, sea-ice expansion, and regional cooling which in turn drove advances of the LIS, GrIS and alpine glaciers. Comparison between the Baffin Bay moraine record and the record of IRD/meltwater through Hudson Strait suggests that this same chain of events likely occurred on several occasions in the early Holocene. The re-occurring relationship between freshwater, AMOC reduction, sea-ice expansion, regional cooling, and response of Baffin Bay ice masses establishes perhaps a fundamental feedback associated with melting ice sheets in the North Atlantic region. Notably, the record of Hudson Strait-sourced IRD and meltwater is similar to a down-current record of IRD included in the original petrologic stack defining early Holocene Bond events, and the complete Bond stack itself (Bond et al., 2001). If IRD recorded at the Cartwright Saddle does indeed reflect the repeated discharge of freshwater through the Hudson Strait as proposed by Jennings et al. (2015), then it is conceivable that early Holocene Bond events are manifestations of regional cooling driven by freshwater injection into the Labrador Sea, AMOC reduction, sea-ice expansion, and attendant southern displacement of the polar front. Nonetheless, the timing of moraine deposition across Baffin Bay, pulses of Hudson Strait-sourced IRD, and episodes of cooling recorded in Greenland Ice cores suggests that, combined, these proxy records serve as a foundational archive of regional climate variability. An overall warming trend was punctuated by freshwater-forced episodes of cooling that drove readvances of the LIS, GrIS, and alpine glaciers during net glacier retreat.

Author contributions

NEY, JPB, GHM, and JMS designed the study. NEY, JPB, GHM, AJL, SEC, and SLP completed significant amounts of fieldwork and sample preparation over the last 10 years. RS, JMS, and NEY oversaw processing and measurement of new ^{10}Be ages and data reporting. NEY wrote the manuscript with input from all co-authors.

Declaration of competing interest

The authors declare that they have no known competing financial interests or personal relationships that could have appeared to influence the work reported in this paper.

Acknowledgements

We thank the Qikiqtaani Inuit and government of Nunavut and Canada for field site access (Nunavut Research Institute license # 02 021 15 R-M; Auyuittuq National Park research permit # ANP-2013-14193). We thank Gordie Audlakiak, Mina Kunilusie, and Allan and Lisa Kunilusie for field support. Parts of this work were supported by the National Science Foundation Arctic Natural Sciences program (Awards #1417675 to NEY and JMS; #1417783 to JPB; #1418040 to GHM) and the Arctic System Sciences program (#1503959 to NEY and JMS; #1504267 to JPB), and CH2MHill Polar Services. We benefited greatly from discussions with Anne Jennings, Jerry McManus, and Paula Reimer regarding certain aspects of this manuscript and who are in no way responsible for this manuscript's remaining shortcomings. Lastly, we thank Vincent Jomelli and an anonymous reviewer for comments that helped improve this manuscript.

Appendix A. Supplementary data

Supplementary data to this article can be found online at https://doi.org/10.1016/j.quascirev.2021.107179.

References

Aguiar, W., Meissner, K.J., Montenegro, A., Prado, L., Wainer, I., Carlson, A.E., Mata, M.M., 2021. Magnitude of the 8.2 ka event freshwater forcing based on stable isotope modelling and comparison to future Greenland melting. Sci. Rep. 11, 5473.
Alley, R.B., Mayewski, P.A., Sowers, T., Stuiver, M., Taylor, K.C., Clark, P.U., 1997. Holocene climatic instability: a prominent, widespread event 8200 yr ago. Geology 25, 483−486.
Alley, R.B., Ágústsdóttir, 2005. The 8k event: causes and consequences of a major Holocene abrupt climate change. Quat. Sci. Rev. 24, 1123−1149.
Alonso-Garcia, M., Kleiven, H.F., McManus, J.F., Moffa-Sanchez, P., Broecker, W.S., Flower, B.J., 2017. Freshening of the Labrador Sea as a trigger for little ice age development. Clim. Past. 13, 317−331.
Andrews, J.T., Drapier, L., 1967. Radiocarbon dates obtained through Geographical Branch field observations. Geogr. Bull. 9, 115−162.
Andrews, J.T., Ives, J., 1978. "Cockburn" nomenclature and the late quaternary history of the eastern Canadian arctic. Arct. Alp. Res. 10, 617−633.
Andrews, J.T., Tedesco, K., 1992. Detrital carbonate-rich sediments, northwestern Labrador sea: implications for ice sheet dynamics and iceberg rafting (Heinrich) events in the North Atlantic. Geology 20, 1087−1090.
Andrews, J.T., Keigwin, L., Hall, F., Jennings, A.E., 1999. Abrupt deglaciation events and Holocene palaeoceanography from high-resolution cores, Cartwright saddle, labrador shelf, Canada. J. Quat. Sci. 14, 383−397.
Andrews, J.T., Barber, D.C., Jennings, A.E., Eberl, D.D., MacLean, B., Kirby, M.E., Stoner, J.S., 2012. Varying sediment sources (Hudson Strait, Cumberland Sound, Baffin Bay) to the NW Labrador Sea slope between and during henirich events 0 to 4. J. Quat. Sci. 27, 475−484.
Applegate, P.J., Urban, N.M., Keller, K., Lowell, T.V., Laabs, B.J.C., Kelly, M.A., Alley, R.B., 2012. Improved moraine age interpretations through explicit matching of geomorphic process models to cosmogenic nuclide measurements from single landforms. Quat. Res. 77, 293−304.
Balascio, N.L., D'Andrea, W.J.D., Bradley, R.S., 2015. glacier response to North Atlantic climate variability during the Holocene. Clim. Past. 11, 1587−1598.
Balco, G., Briner, J., Finkel, R.C., Rayburn, J.A., Ridge, J.C., Schaefer, J.M., 2009. Regional beryllium-10 production rate calibration for late-glacial northeastern North America. Quat. Geochronol. 4, 93−107.
Balco, G., 2020. Glacier change and paleoclimate applications of cosmogenic-nuclide exposure dating. Annu. Rev. Earth Planet Sci. 48, 1.1−1.28.
Barber, D.C., Dyke, A., Hillaire-Marcel, C., Jennings, A.E., Andrews, J.T., Kerwin, M.W., Bilodeau, G., McNeely, R., Southon, J., Morehead, M.D., Gagnon, J.-M., 1999. Forcing of the cold of 8,200 years ago by catastrophic drainage of Laurentide lakes. Nature 400, 344−348.
Barker, S., Chen, J., Gong, X., Jonkers, L., Knorr, G., Thornalley, D., 2015. Icebergs not the trigger for North Atlantic cold events. Nature 520, 333−336.
Bennike, O., 2000. Palaeoecological studies of Holocene lake sediments from west Greenland. Palaeogeogr. Palaeoclimatol. Palaeoecol. 155, 285−304.
Bennike, O., Björck, S., 2002. Chronology of the last recession of the Greenland ice sheet. J. Quat. Sci. 17, 211−219.
Bierman, P., Marsella, K., Patterson, C., Davis, P., Caffee, M., 1999. Mid-Pleistocene cosmogenic minimum-age limits for pre-Wisconsin glacial surfaces in southwestern Minnesota and southern Island, Baffin Island: a multiple nuclide approach. Geomorphology 27, 25−39.
Blake, W., 1966. End moraines and deglaciation chronology in northern Canada, with special reference to southern Baffin Island. Geol. Surv. Can. Pap. 31.
Bond, G., Lotti, R., 1995. Iceberg discharges into the North Atlantic on millennial time scales during the last glaciation. Science 267, 1005−1010.
Bond, G., Heinrich, H., Broecker, W., Labeyrie, L., McManus, J., Andrews, J., Huon, S., Jantschik, R., Clasen, S., Simet, C., Tedesco, K., Klas, M., Bonani, G., Ivy, S., 1992. Evidence for massive discharges of icebergs into the North Atlantic Ocean during the last glacial period. Nature 360, 245−249.
Bond, G., Showers, W., Cheseby, M., Lotti, R., Almasi, P., deMenocal, P., Priore, P., Cullen, H., Hajdas, I., Bonani, G., 1997. A pervasive millennial-scale cycle in North Atlantic Holocene and glacial climates. Science 278, 1257−1266.
Bond, G., Kromer, B., Beer, J., Muscheler, R., Evans, M.N., Showers, W., Hoffmann, S., Lotti-Bond, R., Hajdas, I., Bonani, G., 2001. Persistent solar influence on North Atlantic climate during the Holocene. Science 294, 2130−2136.
Borchers, B., Marrero, S., Balco, G., Caffee, M., Goehring, B., Lifton, N., Nishiizumi, K., Phillips, F., Schaefer, J., Stone, J., 2016. Geological calibration of spallation production rates in the CRONUS-Earth project. Quat. Geochronol. 31, 188−198.
Bradley, R.S., Bakke, J., 2019. Is there evidence for a 4.2 ka BP event in the northern North Atlantic region? Clim. Past. 15, 1665−1676.
Briner, J.B., 2003. The Last Glaciation in the Clyde Region, Northeastern Baffin Island, Arctic Canada: Cosmogenic Isotope Constraints on Laurentide Ice Sheet Dynamics and Chronology [Ph.D. Thesis]. University of Colorado, Boulder, p. 300.
Briner, J.P., Miller, G.H., Davis, P.T., Finkel, R.C., 2006. Cosmogenic radionuclides from fiord landscapes support differential erosion by overriding ice sheets. GSA Bulletin 118, 406−420.
Briner, J.P., Overeem, I., Miller, G., Finkel, R.C., 2007. The deglaciation of Clyde inlet, northeastern Baffin Island, arctic Canada. J. Quat. Sci. 22, 223−232.
Briner, J.P., Bini, A.C., Anderson, R.S., 2009a. Rapid early Holocene retreat of a Laurentide outlet glacier through an Arctic fjord. Nat. Geosci. 2, 496−499. https://doi.org/10.1038/ngeo556.

Briner, J.P., Davis, P.T., Miller, G.H., 2009b. Latest pleistocene and Holocene glaciation of Baffin Island, arctic Canada: key patterns and chronologies. Quat. Sci. Rev. 28, 2075–2087. https://doi.org/10.1016/j.quascirev.2008.09.017.
Briner, J.P., Young, N.E., Goehring, B.M., Schaefer, J.M., 2012. Constraining Holocene ^{10}Be production rates in Greenland. J. Quat. Sci. 27, 2–6.
Broecker, W., Bond, G., Klas, M., Clark, E., McManus, J., 1992. Origin of the northern Atlantic's Heinrich events. Clim. Dynam. 6, 265–273.
Broecker, W., Sutherland, S., Peng, T.-H., 2001. A possible 20th-century slowdown of Southern Ocean deep water formation. Science 286, 1132–1135.
Bronk Ramsey, C., 2009. Bayesian analysis of radiocarbon dates. Radiocarbon 51, 337–360.
Buizert, C., Gkinis, V., Severinghaus, J.P., He, F., Lecavalier, B.S., Kindler, P., Meuenberger, M., Carlson, A.E., Vinther, B., Masson-Delmotte, V., White, J.W.C., Liu, Z., Otto-Bliesner, B., Brook, E.J., 2014. Greenland temperature response to climate forcing during the last deglaciation. Science 345, 1177–1180.
Carlson, A.E., Winsor, K., Ullman, D.J., Brook, E.J., Rood, D.H., Axford, Y., LeGrande, A.N., Anslow, F.S., Sinclair, G., 2014. Earliest Holocene south Greenland ice sheet retreat within its late Holocene extent. Geograph. Res. Lett. 41. https://doi.org/10.1002/2014GL060800.
Ceperley, E.G., Marcott, S.A., Reusche, M.M., Barth, A.M., Mix, A.C., Brook, E.J., Caffee, M., 2020. Widespread early Holocene deglaciation, Washington Lane, northwest Greenland. Quat. Sci. Rev. 231, 106181.
Cheng, H., Sinha, A., Verheyden, S., Nader, F.H., Li, X.L., Zhang, P.Z., Yin, J.J., Yi, L., Peng, Y.B., Gao, Z.G., Ning, Y.F., Edwards, R.L., 2015. The climate variability in northern Levant over the past 20,000 years. Geophys. Res. Lett. 42, 8641–8650.
Chmeleff, J., von Blanckenburg, F., Lossert, K., Jakob, D., 2010. Determination of the ^{10}Be half-life by multicollector icp-ms and liquid scintillation counting. *Nucl. Instrum. Methods Phys*. Res. B. 268, 192–199.
Condron, A., Winsor, P., 2011. A subtropical fate awaited freshwater discharged from glacial Lake Agassiz. Geophys. Res. Lett. 38, L03705. https://doi.org/10.1029/2010GL046011.
Corbett, L.B., Young, N.E., Bierman, P.R., Briner, J.P., Neumann, T.A., Rood, D.H., Graly, J.A., 2011. Paired bedrock and boulder ^{10}Be concentrations resulting from early Holocene ice retreat near Jakobshavn Isfjord, western Greenland. Quat. Sci. Rev. 30, 1739–1749.
Corbett, L.B., Bierman, P.R., Davis, P.T., 2016. Glacial history and landscape evolution of southern Cumberland Peninsula, Baffin Island, Canada, constrained by cosmogenic ^{10}Be and ^{26}Al. GSA Bulletin 128, 1173–1192.
Cowan, B., 2015. Shorelines beneath the Sea: Geomorphology and Characterization of the Post-glacial Sea-Level Lowstand, Cumberland Peninsula, Baffin Island, Nunavut. MSc Thesis. Memorial University of Newfoundland and Labrador, p. 332.
Cronauer, S.L., Briner, J.P., Kelley, S.E., Zimmerman, S.R.H., Morlighem, M., 2016. ^{10}Be dating reveals early-middle Holocene age of the Drygalski Moraines in central West Greenland. Quat. Sci. Rev. 147, 59–68.
Crump, S.E., Anderson, L.S., Miller, G.H., Anderson, R.S., 2017. Interpreting exposure ages from ice- cored moraines: a Neoglacial case study on Baffin Island, Arctic Canada. J. Quat. Sci. 32, 1049–1062. https://doi.org/10.1002/jqs.2979.
Crump, S.E., Young, N.E., Miller, G.H., Pendleton, S.L., Tulenko, J.P., Anderson, R.S., Briner, J.P., 2020. Glacier expansion on Baffin Island during early Holocene cold reversals. Quat. Sci. Rev. 241, 106419.
Dansgaard, W., Johnsen, S., Clausen, H., Langway, C., 1971. Climatic record revealed by the Camp Century ice core. In: Turekian, K.K. (Ed.), The Late Cenezoic Glacial Ages. Yale University Press, New Haven, pp. 37–56.
Davis, P.T., Briner, J.P., Coulthard, R.D., Finkel, R.C., Miller, G.H., 2006. Preservation of Arctic landscapes overridden by cold-based ice sheets. Quat. Res. 65, 156–163.
Debret, M., Bout-Roumazeilles, V., Grousset, F., Desmet, M., McManus, J.F., Massei, N., Sebag, D., Petit, J.-R., Copard, Y., Trentesaux, A., 2007. The origin of the 1500-year climate cycle in Holocene North-Atlantic records. Clim. Past. 3, 569–575.
Denton, G.H., Alley, R.B., Comer, G.C., Broecker, W.S., 2005. The role of seasonality in abrupt climate change. Quat. Sci. Rev. 24, 1159–1182.
Donner, J., Junger, H., 1975. Radiocarbon dating of shells from marine Holocene deposits in the Disko Bugt area, west Greenland. Boreas 4, 24–45.
Dredge, L.A., 2004. Surficial geology, McBeth fiord (west half), central Baffin Island, Nunavut. Geological Survey of Canada. Map 2074A, scale 1:250,000.
Dyke, A.S., 1979. Glacial and sea-level history of southwestern Cumberland Peninsula, Baffin Island, N.W.T., Canada. Arct. Alp. Res. 11, 179–202.
Dyke, A.S., 2004. An outline of North American Deglaciation with emphasis on central and northern Canada. In: Ehlers, J., Gibbard, P.L. (Eds.), Quaternary Glaciations-Extent and Chronology Part II, vol. 2b. Elsevier, Amsterdam, pp. 371–406.
Falconer, G., Andrews, J.T., Ives, J.D., 1965. Late-Wisconsin end moraines in Northern Canada. Science 147, 608–610.
Forbes, D.L., Cowan, B., Muggah, J., Hirogi, A., Bell, T., 2012. M.V. Nuliajuk cruise report: Clyde river to pangnirtung, NU. Memorial University of Newfoundland. Oct. 3-19, 2012.
Fratantoni, P.S., McCartney, M.S., 2010. Freshwater export from the labrador current to the North atlantic current at the tail of the grand banks of Newfoundland. Deep-Sea Res. I 57, 258–283.
Fredskild, B., 1983. Holocene vegetational development of the Godthåbsfjord area, West Greenland. Meddelelser Om Grønland Geoscience 10, 1–28.
Funder, S., Kjellerup, K., Kjær, K.H., Ó Cofaigh, C., 2011. The Greenland ice sheet during the last 300,000 years: a review. In: Ehlers, J., Gibbard, P., Hughes, P.D. (Eds.), Quaternary Glaciations—Extent and Chronology: A Closer Look: Developments in Quaternary Science.
Garcia, J.L., Kaplan, M.R., Hall, B.L., Schaefer, J.M., Vega, R.M., Schwartz, R., Finkel, R., 2012. Glacier expansion in southern Patagonia throughout the Antarctic cold reversal. Geology 40, 859–862.
Gardner, A., Moholdt, G., Arendt, A., Wouters, B., 2012. Accelerated contributions of Canada's Baffin and Bylot Island glaciers to sea level rise over the past half century. Cryosphere 6, 1103–1125.
Gauthier, M.S., Kelley, S.E., Hodder, T.J., 2020. Lake agassiz drainage bracketed Holocene Hudson Bay ice saddle collapse. Earth Planet Sci. Lett. 544, 116372.
Gibbons, A.B., Megeath, J.D., Pierce, K.L., 1984. Probability of moraine survival in a succession of glacial advances. Geology 12, 327–330. https://doi.org/10.1130/0091-7613(1984)12<327:POMSIA>2.0.CO;2.
Gosse, J.C., Klein, J., Evenson, E.B., Lawn, B., Middleton, R., 1995a. Beryllium-10 dating of the duration and retreat of the last Pinedale glacial sequence. Science 268, 1329–1333.
Gosse, J.C., Evenson, E.B., Klein, J., Lawn, B., Middleton, R., 1995b. Precise cosmogenic ^{10}Be measurements in western North America: support for a global Younger Dryas cooling event. Geology 23, 877–880.
Granger, D.E., Lifton, N.A., Willenbring, J.K., 2013. A cosmic trip: 25 years of cosmogenic nuclides in geology. GSA Bulletin 125, 1379–1402.
Heaton, T.J., Köhler, P., Butzin, M., Bard, E., Reimer, R.W., Austin, W.E.N., Bronk Ramsey, C., Grootes, P.M., Hughen, K.A., Kromer, B., Reimer, P.J., Adkins, J., Burke, A., Cook, M.S., Olsen, J., Skinner, L.C., 2020. Marine20-The marine radiocarbon age calibration curve (0-55,000 cal BP). Radiocarbon 62, 779–820. https://doi.org/10.1017/RDC.2020.68.
Hillaire-Marcel, C., de Vernal, A., Piper, D.J.W., 2007. Lake Agassiz final drainage event in the northwest North Atlantic. Geophys. Res. Lett. 34, L15601.
Hu, F.S., Kaufman, D., Yoneji, S., Nelson, D., Shemesh, A., Huang, Y., Tian, J., Bond, G., Clegg, B., Brown, T., 2003. Cyclic variation and solar forcing of Holocene climate in the Alaskan subarctic. Science 301, 1890–1893.
Ives, J.D., 1978. The maximum extent of the Laurentide Ice Sheet along the east coast of North America during the last glaciation. Arctic 31, 24–53.
Ives, J.D., Andrews, J.T., 1963. Studies in the physical geography of north-central Baffin Island. N.W.T. *Geogr. Bull*. 19, 5–48.
Jennings, A.E., 1993. The quaternary history of Cumberland Sound, southeastern Baffin Island: the marine evidence. Géogr. Phys. Quaternaire 47, 21–42.
Jennings, A.E., Tedesco, K.A., Andrews, J.T., Kirby, M.E., 1996. Shelf erosion and glacial ice proximity in the Labrador Sea during and after Heinrich events (H-3 or 4 to H-0) as shown by foraminifera. In: Andrews, J.T., et al. (Eds.), Late Quaternary Paleoceanography of the North Atlantic Margins, vol. 111. Geological Society (London) Special Publication, pp. 29–49.
Jennings, A., Andrews, J., Pearce, C., Wilson, L., Olfasdotttir, S., 2015. Detrital carbonate peaks on the Labrador shelf, a 13-7 ka template for freshwater forcing from the Hudson Strait outlet of the Laurentide Ice Sheet into the subpolar gyre. Quat. Sci. Rev. 107, 62–80.
Kaplan, M.R., Miller, G.H., Steig, E.J., 2001. Low-gradient outlet glaciers (ice streams?) drained the Laurentide ice sheet. Geology 29, 343–346.
Kaplan, M.R., Schaefer, J.M., Denton, G.H., Barrell, D.J.A., Chinn, T.J.H., Putnam, A.E., Andersen, B.G., Finkel, R.C., Schwartz, R., Doughty, A.M., 2010. glacier retreat in New Zealand during the younger Dryas stadial. Nature 467, 194–197.
Kaplan, M.R., Strelin, J.A., Schaefer, J.M., Denton, G.H., Finkel, R.C., Schwartz, R., Putnam, A.E., Vandergoes, M.J., Goehring, B.M., Travis, S.G., 2011. In-situ cosmogenic 10Be production rate at Lago Argentino, Patagonia: implications for late-glacial climate chronology. Earth Planet Sci. Lett. 309, 21–32.
Kaplan, M.R., Schaefer, J.M., Denton, G.H., Doughty, A.M., Barrell, D.J.A., Chinn, T.J.H., Putnam, A.E., Andersen, B.G., Mackintosh, A., Finkel, R.C., Schwartz, R., Anderson, B., 2013. The anatomy of long-term warming since 15 ka in New Zealand based on net glacier snowline rise. Geology 41, 887–890.
Kelley, S.E., Briner, J.P., Young, N.E., 2013. Rapid ice retreat in Disko Bugt supported by ^{10}Be dating of the last recession of the western Greenland Ice Sheet. Quat. Sci. Rev. 82, 13–22.
Kelley, S.E., Briner, J.P., Zimmerman, S.R.H., 2015. The influence of ice marginal setting on early Holocene retreat rates in central West Greenland. J. Quat. Sci. 30, 271–280.
Kelly, M., 1985. A review of the Quaternary Geology of western Greenland. In: Andrews, J.T. (Ed.), Quaternary Environments Eastern Canadian Arctic, Baffin Bay, Western Greenland. Allen & Unwin, Boston, pp. 461–501.
Kelly, M.A., Lowell, T.V., Hall, B.L., Schaefer, J.M., Finkel, R.C., Goehring, B.M., Alley, R.B., Denton, G.H., 2008. A 10Be chronology of lateglacial and Holocene mountain glaciation in the Scoresby Sund region, east Greenland: implications for seasonality during lateglacial time. Quat. Sci. Rev. 27, 2273–2282.
Kelly, M.A., Lowell, T.V., Applegate, P.J., Phillips, F.M., Schaefer, J.M., Smith, C.A., Kim, H., Leonard, K.C., Hudson, A.M., 2015. A locally calibrated, late glacial 10Be production rate from a low-latitude, high-altitude site in the Peruvian Andes. Quat. Geochronol. 26, 70–85.
Kobashi, T., Severinghaus, J.P., Brook, E.J., Barnoa, J.-M., Grachev, A.M., 2007. Precise timing and characterization of abrupt climate change 8200 years ago from air trapped in polar ice. Quat. Sci. Rev. 26, 1212–1222.
Kobashi, T., Menviel, L., Jeltsch-Thömmes, A., Vinther, B.M., Box, J.E., Muscheler, R., Nakaegawa, T., Pfister, P.L., Döring, M., Leuenberger, M., Wanner, H., Ohmura, A., 2017. Volcanic influence on centennial to millennial Holocene Greenland temperature change. Sci. Rep. 7, 1441. https://doi.org/10.1038/s41598-017-0451-7.
Lal, D., 1991. Cosmic ray labeling of erosion surfaces: in situ nuclide production rates and erosion models. Earth Planet Sci. Lett. 104, 424–429.
Larsen, N.K., Kjær, K.H., Lecavalier, B., Bjørk, A.A., Colding, S., Huybrechts, P.,

Jakobsen, K.E., Kjeldsen, K.K., Knudsen, K.-L., Odgaard, B.V., Olsen, J., 2015. The response of the southern Greenland ice sheet to the Holocene thermal maximum. Geology 43, 291–294.
LeGrande, A.N., Schmidt, G.A., 2008. Ensemble, water isotope-enabled, coupled general circulation modeling insights into the 8.2 ka event. Paleoceanography 23, PA3207.
Lesnek, A.J., Briner, J.P., 2018. Response of a land-terminating sector of the western Greenland Ice Sheet to early Holocene climate change: evidence from ^{10}Be dating in the Søndre Isortoq region. Quat. Sci. Rev. 180, 145–156.
Lesnek, A.J., Briner, J.P., Young, N.E., Cuzzone, J.K., 2020. Maximum Southwest Greenland Ice Sheet recession in the early Holocene. Geophys. Res. Lett. 47 e2019GL083164.
Levy, L.B., Kelly, M.A., Howley, J.A., Virginia, R.A., 2012. Age of the ørkendalen moraines, Kangerlussuaq, Greenland: constraints on the extent of the southwestern margin of the Greenland ice sheet during the Holocene. Quat. Sci. Rev. 52, 1–5.
Levy, L.B., Kelly, M.A., Lowell, T.V., Hall, B.L., Howley, J.A., Smith, C.A., 2016. Coeval fluctuations of the Greenland ice sheet and a local glacier, central East Greenland, during late glacial and early Holocene time. Geophys. Res. Lett. 43, 1623–1631.
Levy, L.B., Kelly, M.A., Applegate, P.A., Howley, J.A., Virginia, R.A., 2018. Middle to late Holocene chronology of the western margin of the Greenland Ice Sheet: a comparison with Holocene temperature and precipitation records. Arct. Antarct. Alp. Res. 50, 1414477.
Lewis, C.F.M., Miller, A.A.L., Levac, E., Piper, D.J.W., Sonnichsen, G.V., 2012. Lake Agassiz outburst age and routing by Labrador Current and the 8.2 cal ka cold event. Quat. Intl. 260, 83–97.
Li, C., Born, A., 2019. Coupled atmosphere-ice-ocean dynamics in Dansgaard-Oeschger events. *Quat. Sci. Rev.* 203, 1–20.
Licciardi, J.M., Clark, P.U., Brook, E.J., Pierce, K.L., Kruz, M.D., Elmore, D., Sharma, P., 2001. Cosmogenic ^{3}He and ^{10}Be chronologies of the late Pinedale northern Yellowstone ice cap, Montana, USA. Geology 29, 1095–1098.
Lloyd, J., et al., 2005. Early Holocene palaeoceanography and deglacial chronology of Disko Bugt , West Greenland. Quat. Sci. Rev. 24, 1741–1755.
Long, A.J., Roberts, D.H., 2002. A revised chronology for the 'Fjord Stade' moraine in Disko Bugt, west Greenland. J. Quat. Sci. 17, 561–579.
Long, A.J., Roberts, D.H., Rasch, M., 2003. New observations on the relative sea level and deglacial history of Greenland from Innaarsuit. Disko Bugt. *Quat. Res.* 60, 162–171.
Long, A.J., Roberts, D.H., Dawson, S., 2006. Early Holocene history of the west Greenland ice sheet and GH-8.2 event. Quat. Sci. Rev. 25, 904–922.
Lowell, T.V., Hayward, R.K., Denton, G.H., 1999. Role of climate oscillations in determining ice-margin positions: hypothesis, examples, implications. In: Mickleson, D.M., Attig, J.W. (Eds.), Glacial Processes Past and Present, vol. 337. Geological of Society of America Special Paper, Boulder, CO.
Lund, D.C., Lynch-Stieglitz, J., Curry, W.B., 2006. Gulf Stream density structure and transport during the past millennium. Nature 444, 601–604.
Marcott, S.A., Clark, P.U., Shakun, J.D., Brook, E.J., Davis, P.T., Caffee, M.W., 2019. ^{10}Be age constraints on latest Pleistocene and Holocene cirque glaciation across the western United States. npj Climate and Atmospheric Science 2, 5. https://doi.org/10.1038/s41612-019-0062-z.
Margreth, A., Gosse, J.C., Dyke, A.S., 2017. Wisconsinan and early Holocene glacial dynamics of Cumberland peninsula, Baffin Island, arctic Canada. *Quat. Sci.* Rev. 168, 79–100. https://doi.org/10.1016/j.quascirev.2017.04.033.
Margreth, A., Gosse, J.C., Dyke, A.S., 2016. Quantification of subaerial and episodic subglacial erosion rates on high latitude upland plateaus: Cumberland Peninsula, Baffin Island, Arctic Canada. *Quat. Sci. Rev.* 133, 108–129. https://doi.org/10.1016/j.quascirev.2015.12.017.
Marsella, K.A., Bierman, P.R., Davis, P.T., Caffee, M.W., 2000. Cosmogenic ^{10}Be and ^{26}Al ages for the last glacial maximum, eastern Baffin Island, arctic Canada. GSA Bulletin 112, 1296–1312.
Martin, L.C.P., Blard, P.-H., Lavé, J., Braucher, R., Lupker, M., Condom, T., Charreau, J., Mariotti, V., , ASTER Team, Davy, E., 2015. In situ cosmogenic 10Be production rate in the High Tropical Andes. Quat. Geochronol. 30, 54–68.
Martin, L.C.P., Blard, P.-H., Lavé, J., Jomelli, V., Charreau, J., Condom, T., Lupker, M., ASTER Team, 2020. Antarctic-like temperature variations in the Tropical Andes recorded by glaciers and lakes during the last deglaciation. Quat. Sci. Rev. 247, 106542.
Matero, I.S.O., Gregoire, L.J., Ivanovic, R.F., Tindall, J.C., Haywood, A.M., 2017. The 8.2 ka cooling event caused by Laurentide ice saddle collapse. Earth Planet Sci. Lett. 473, 205–214.
McManus, J.F., Oppo, W.D., Cullen, J.L., 1999. A 0.5-million-year record of millennial-scale climate variability in the North Atlantic. Science 283, 971–974.
Miller, G.H., Dyke, A.S., 1974. Proposed extent of late Wisconsin Laurentide ice on eastern Baffin Island. Geology 2, 125–130.
Miller, G.H., 1975. Glacial and Climatic History of Northern Cumberland Peninsula, Baffin Island, Canada, during the Last 10,000 Years. University of Colorado, Department of Geological Sciences, Boulder [Ph.D. thesis].
Miller, G.H., Wolfe, A.P., Steig, E.J., Sauer, P.E., Kaplan, M.R., Briner, J.P., 2002. The Goldilocks dilemma: big ice, little ice, or "just-right" ice in the eastern Canadian Arctic. Quat. Sci. Rev. 21, 33–48.
Miller, G.H., Lehman, S.J., Refsnider, K.A., Southon, J.R., Zhong, Y., 2013. Unprecedented recent summer warmth in Arctic Canada. Geophys. Res. Lett. 40, 5745–5751.
Morrill, C., LeGrande, A.N., Renssen, H., Bakker, P., Otto-Bliesner, B.L., 2013. Model sensitivity to North Atlantic freshwater forcing at 8.2 ka. Clim. Past. 9, 955–968.
Nishiizumi, K., Imamura, M., Caffee, M.W., Southon, J.R., Finkel, R.C., McAninch, J., 2007. Absolute calibration of ^{10}Be AMS standards. Nucl. Instrum. Methods Phys. Res. B 258, 403–413.
O'Hara, S.L., Briner, J.P., Kelley, S.E., 2017. A ^{10}Be chronology of early Holocene local glacier moraines in central West Greenland. Boreas 46, 655–666.
Pendleton, S.L., Miller, G.H., Lifton, N., Lehman, S.J., Southon, J., Crump, S.E., Anderson, R.S., 2019. Rapidly receding Arctic Canada glaciers revealing landscapes continuously ice-covered for more than 40,000 years. Nat. Commun. 10. https://doi.org/10.1038/s41467-019-08307-w.
Putnam, A.E., Schaefer, J.M., Barrell, D.J.A., Vandergoes, M., Denton, G.H., Kaplan, M.R., Finkel, R.C., Schwartz, R., Goehring, B.M., Kelley, S.E., 2010a. In situ cosmogenic 10Be production-rate calibration from the Southern Alps, New Zealand. Quat. Geochronol. 5, 392–409.
Putnam, A.E., Denton, G.H., Schaefer, J.M., Barrell, D.J.A., Andersen, B.G., Finkel, R.C., Schwartz, R., Doughty, A.M., Kaplan, M.R., Schlüchter, C., 2010b. glacier advance in southern middle-latitudes during the antarctic cold reversal. Nat. Geosci. 3, 700–704.
Putnam, A.E., Schaefer, J.M., Denton, G.H., Barrell, D.J.A., Finkel, R.C., Andersen, B.G., Schwartz, R., Chinn, T.J.H., Doughty, A.M., 2012. Regional climate control of glaciers in New Zealand and Europe during the pre-industrial Holocene. Nat. Geosci. 5, 627–630.
Putnam, A.E., Bromely, G.R.M., Rademaker, K., Schaefer, J.M., 2019. In situ ^{10}Be production-rate calibration from a ^{14}C-dated late-glacial moraine belt in Rannoch Moor, central Scottish Highlands. Quat. Geochronol. 50, 109–125.
Rashid, H., Piper, D.J., Flower, B.P., 2011. The role of Hudson Strait outlet in younger Dryas sedimentation in the Labrador Sea. Abrupt climate change: mechanisms, patterns, and impacts. In: Geophysical Monograph Series 193. American Geophysical Union.
Reimer, P.J., Austin, W.E.N., Bard, E., Bayliss, A., Blackwell, P.G., Bronk Ramsey, C., Cheng, H., Edwards, R.L., Friedrich, M., Grootes, P.M., Guilderson, T.P., Hajdas, I., Heaton, T.J., Hogg, A.G., Hughen, K.A., Kromer, B., Manning, S.W., Muscheler, R., Palmer, J.G., Pearson, C., van der Plicht, J., Reimer, R.W., Richards, D.A., Scott, E.M., Southon, J.R., Turney, C.S.M., Wacker, L., Adolphi, F., Büntgen, U., Capano, M., Fahrni, S.M., Fogtmann-Schulz, A., Friedrick, R., Köhler, P., Kudsk, S., Miyake, F., Olsen, J., Reinig, F., Sakamoto, M., Sookdeo, A., Talamo, S., 2020. INTCAL20 Northern Hemisphere radiocarbon age calibration curve (0-55 CAL kBP). Radiocarbon 62, 725–757. https://doi.org/10.1017/RDC.2020.41.
Reusche, M.M., Marcott, S.A., Ceperley, E.G., Barth, A.M., Brook, E.J., Mix, A.C., Caffee, M.W., 2018. Early to late Holocene surface exposure ages from two marine-terminating outlet glaciers in Northwest Greenland. Geophys. Res. Lett. 45. https://doi.org/10.1029/2018GL078266.
Reverdin, G., Niiler, P.P., Valdimarsson, H., 2003. North Atlantic Ocean surface currents. *J. Geophys. Res.* 108, 3002.
Rinterknecht, V., Gorokhovich, Y., Schaefer, J., Caffee, M., 2009. Preliminary ^{10}Be chronology for the last deglaciation of the western margin of the Greenland Ice Sheet. J. Quat. Sci. 24, 270–278.
Roberts, D.H., Long, A.J., Schnabel, C., Davies, B.J., Xu, S., Simpson, M.J.R., Huybrechts, P., 2009. Ice sheet extent and early deglacial history of the southwestern sector of the Greenland Ice Sheet. Quat. Sci. Rev. 28, 2760–2773.
Roe, G.H., 2011. What do glaciers tell us about climate variability and climate change? J. Glaciol. 57, 567–578.
Roksandic, M.M., 1979. Geology of the continental shelf off West Greenland between 61°15′N and 64°00′N: an interpretation of sparker seismic and echo sounder data. Grønlands Geol. Unders. 92, 15pp.
Rood, D.H., Hall, S., Guilderson, T.P., Finkel, R.C., Brown, T.A., 2010. Challenges and opportunities in high-precision Be-10 measurements at CAMS. Nucl. Instrum. Methods Phys. Res. B 268, 730–732.
Rood, D.H., Brown, T.A., Finkel, R.C., Guilderson, T.P., 2013. Poisson and non-Poisson uncertainty estimations of ^{10}Be/^{9}Be measurements at LLNL-CAMS. Nucl. Instrum. Methods Phys. Res. B 294, 426–429.
Roy, M., Dell'Oste, F., Veillette, J.J., de Vernal, A., Hélie, J.-F., Parent, M., 2011. Insights on the events surrounding the final drainage of Lake Ojibway based on James Bay stratigraphic sequences. Quat. Sci. Rev. 30, 682–692.
Schaefer, J.M., Denton, G.H., Kaplan, M., Putnam, A., Finkel, R.C., Barrell, D.J.A., Andersen, B.G., Schwartz, R., Mackintosh, A., Chinn, T., Schlüchter, C., 2009. High-frequency Holocene glacier fluctuations in New Zealand differ from the northern signature. Science 324, 622–625.
Staiger, J., Gosse, J., Toracinta, R., Oglesby, B., Fastook, J., Johnson, J.V., 2007. Atmospheric scaling of cosmogenic nuclide production: climate effect. J. Geophys. Res. 112, 2205.
Stone, J.O., 2000. Air pressure and cosmogenic isotope production. J. Geophys. Res. 105, 23,753–23,759.
Storms, J.E.A., de Winter, I.J., Overeem, I., Drijkoningen, G.G., Lykke-Andersen, H., 2012. The Holocene sedimentary history of the Kangerlussuaq fjord-valley fill, west Greenland. Quat. Sci. Rev. 35, 29–50.
Sugden, D.E., 1978. Glacial erosion by the Laurentide ice sheet. J. Glaciol. 83, 367–391.
Ten Brink, N.W., 1975. Holocene history of the Greenland Ice Sheet based on radiocarbon-dated moraines in west Greenland. Meddelelser om Grønland 44, 113.
Ten Brink, N.W., Weidick, A., 1974. Greenland Ice Sheet history since the last glaciation. *Quat. Res.* 4, 429–440.
Thomas, E.K., Szymanski, J., Briner, J.P., 2010. Holocene alpine glaciation inferred from lacustrine sediments on northeastern Baffin Island, Arctic Canada. J. Quat.

Sci. 25, 146–161.
Ullman, D.J., Carlson, A.E., Hostetler, S.W., Clark, P.U., Cuzzone, J., Milne, G.A., Winsor, K., Caffee, M., 2016. Final Laurentide ice-sheet deglaciation and Holocene climate-sea level change. Quat. Sci. Rev. 152, 49–59.
van Tatenhove, F.G., van der Meer, J.J., Koster, E.A., 1996. Implications for deglaciation chronology from new AMS age determinations in central West Greenland. Quat. Res. 45, 245–253.
Wagner, A.J., Morrill, C., Otto-Bliesner, B.L., Rosenbloom, N., Watkins, K.R., 2013. Model support for forcing of the 8.2 ka event by meltwater from the Hudson Bay ice dome. Clim. Dynam. 41, 2855–2873.
Wang, Y., Cheng, H., Edwards, R.L., He, Y., Kong, X., An, Z., Wu, J., Kelly, M.J., Dykoski, C.A., Li, X., 2005. The Holocene asian monsoon: links to solar changes and North atlantic climate. Science 308, 854–857.
Wanner, H., Bütikofer, J., 2008. Holocene Bond cycles: real or imaginary? Geographie 113, 338–350.
Wanner, H., Solomina, O., Grosjean, M., Ritz, S.P., Jetel, M., 2011. Structure and origin of Holocene climate events. Quat. Sci. Rev. 30, 3109–3123.
Warren, C.R., Hulton, N.R.J., 1990. Topographic and glaciological controls on Holocene ice-sheet margin dynamics, central West Greenland. Ann. Glaciol. 14, 307–310.
Weidick, A., 1968. Observations on Some Holocene Glacier Fluctuations in West Greenland: *Meddelelser Om Grønland*, vol. 165, p. 202.
Weidick, A., 1972a. C^{14} dating of survey material performed in 1971. Rapp. - Grnl. Geol. Undersgelse 45, 58–67.
Weidick, A., 1972b. Holocene shore-lines and glacial stages in Greenland – an attempt at correlation. Rapp. - Grnl. Geol. Undersgelse 41, 1e39.
Weidick, A., 1972c. Notes on Holocene glacial events in Greenland. Acta Univ. Ouluensis - Ser. A Sci. Rerum Nat. 3, 177–204.
Weidick, A., 1973. C^{14} dating of survey material performed in 1972. Rapp. - Grnl. Geol. Undersgelse 55, 66–75.
Weidick, A., 1974a. C^{14} dating of survey material performed in 1973. Rapp. - Grnl. Geol. Undersgelse 66, 42–45.
Weidick, A., 1974b. Quaternary map of Greenland, 1:500 000, Søndre strømfjord – nûgssuaq. Geological Survey of Greenland, Copenhagen.
Weidick, A., 1975. C^{14} dating of survey material performed in 1974. Rapp. - Grnl. Geol. Undersgelse 75, 19–20.
Weidick, A., 1976. C^{14} dating of survey material, carried out in 1975. Rapp. - Grnl. Geol. Undersgelse 80, 136–144.
Weidick, A., Bennike, O., 2007. Quaternary glaciation history and glaciology of Jakobshavn Isbræ and the Disko Bugt region, west Greenland: a review. Geol. Surv. Den. Greenl. Bull. 14, 1–78.
Weidick, A., Bennike, O., Citterio, M., Nørgaard-Pedersen, N., 2012. Neoglacial and historical glacier changes around Kangersuneq fjord in southern West Greenland. Geol. Surv. Den. Greenl. Bull. 27, 1–68.
Winsor, K., Carlson, A.E., Caffee, M.W., Rood, D.H., 2015. Rapid last-deglacial thinning and retreat of the marine-terminating southwestern Greenland ice sheet. Earth Planet Sci. Lett. 426, 1–12.
Young, N.E., Briner, J.P., 2015. Holocene evolution of the western Greenland Ice Sheet: assessing geophysical ice-sheet models with geological reconstructions of ice-margin change. Quat. Sci. Rev. 114, 1–17.
Young, N.E., Briner, J.P., Stewart, H.A.M., Axford, Y., Csatho, B., Rood, D.H., Finkel, R.C., 2011a. Response of Jakobshavn isbrae Greenland, to Holocene climate change. Geology 39, 131–134.
Young, N.E., Briner, J.P., Axford, Y., Csatho, B., Babonis, G.S., Rood, D.H., Finkel, R.C., 2011b. Response of a marine-terminating Greenland outlet glacier to abrupt cooling 8200 and 9300 years ago. Geophs. Res. Lett. 38, L24701. https://doi.org/10.1029/2011GL049639.
Young, N.E., Briner, J.P., Leonard, E.M., Licciardi, J.M., Lee, K., 2011c. Assessing climatic and nonclimatic forcing of Pinedale glaciation and deglaciation in the western United States. Geology 39, 171–174.
Young, N.E., Briner, J.P., Rood, D.H., Finkel, R.C., 2012. glacier extent during the younger Dryas and 8.2-ka event on Baffin Island, arctic Canada. Science 337, 1330–1333.
Young, N.E., Briner, J.P., Rood, D.H., Finkel, R.C., Corbett, L.B., Bierman, P.R., 2013a. Age of the Fjord Stade moraines in the Disko Bugt region, western Greenland, and the 9.3 and 8.2 ka cooling events. Quat. Sci. Rev. 60, 76–90.
Young, N.E., Schaefer, J.M., Briner, J.P., Goehring, B.M., 2013b. A ^{10}Be production-rate calibration for the Arctic. J. Quat. Sci. 28, 515–526.
Young, N.E., Schaefer, J.M., Goehring, B., Lifton, N., Schimmelpfennig, I., Briner, J.P., 2014. West Greenland and global in situ ^{14}C production-rate calibrations. J. Quat. Sci. 29, 401–406.
Young, N.E., Schweinsberg, A.D., Briner, J.P., Schaefer, J.M., 2015. Glacier maxima in Baffin Bay during the medieval warm period coeval with norse settlement. Sci. Adv. 1, 1500806.
Young, N.E., Briner, J.P., Maurer, J., Schaefer, J., 2016. ^{10}Be measurements in bedrock constrain erosion beneath the Greenland Ice Sheet margin. Geophys. Res. Lett. 43. https://doi.org/10.1002/2016GL070258.
Young, N.E., Briner, J.P., Schaefer, J., Zimmerman, S., Finkel, R.C., 2019. Early Younger Dryas glacier culmination in southern Alaska: implications for North Atlantic climate change during the last deglaciation. Geology 47, 550–554.
Young, N.E., Briner, J.P., Miller, G.H., Lesnek, A.J., Crump, S.E., Thomas, E.K., Pendleton, S.L., Cuzzone, J., Lamp, J., Zimmerman, S., Caffee, M., Schaefer, J.M., 2020a. Deglaciation of the Greenland and Laurentide ice sheets interrupted by glacier advance during abrupt coolings. Quat. Sci. Rev. 229, 106091.
Young, N.E., Briner, J.P., Miller, G.H., Lesnek, A.J., Crump, S.E., Thomas, E.K., Pendleton, S.L., Cuzzone, J., Lamp, J., Zimmerman, S., Caffee, M., Schaefer, J.M., 2020b. Reply to Carlson (2020) comment on "Deglaciation of the Greenland and Laurentide ice sheets interrupted by glacier advance during abrupt coolings. Quat. Sci. Rev. 240, 106329.
Young, N.E., Lesnek, A.J., Cuzzone, J.K., Briner, J.P., Badgeley, J.A., Balter-Kennedy, A., Graham, B.L., Cluett, A., Lamp, J.L., Schwartz, R., Tuna, T., Bard, E., Caffee, M.W., Zimmerman, S.R.H., Schaefer, J.M., 2021. In situ cosmogenic 10Be-14C-26Al measurements from recently deglaciatedbedrock as a new tool to decipher changes in Greenland Ice Sheet size. Clim. Past. 17, 419–450. https://doi.org/10.5194/cp-17-419-2021.
Yu, S.-Y., Colman, S.M., Lowell, T.V., Milne, G.A., Fischer, T.G., Breckenridge, A., Boyd, M., Teller, J.T., 2010. Freshwater outburst from Lake Superior as a trigger for the cold event 9300 years ago. Science 328, 1262–1266.
Zielhofer, C., Köhler, A., Mischke, S., Benkaddour, A., Mikdad, A., Flethcer, W.J., 2019. WesternMediterranean hydro-climate consequences of Holocene ice-rafted debris (Bond) events. Clim. Past. 15, 463–475.